รายงานวิจัยฉบับสมบูรณ์

# การเตรียมเซรามิก BNT-BKT-KNN ด้วยวิธีการเผาไหม้

# Preparation of BNT-BKT-KNN via Combustion Method

ผศ.ดร.ธีระชัย บงการณ์
ภาควิชาฟิสิกส์ คณะวิทยาศาสตร์ มหาวิทยาลัยนเรศวร



สนับสนุนโดยกองทุนวิจัยมหาวิทยาลัยนเรศวร

## กิตติกรรมประกาศ

งานวิจัยนี้ได้รับการสนับสนุนงบประมาณจากกองทุนวิจัยมหาวิทยาลัยนเรศวร ผู้วิจัยและคณะขอขอบพระคุณ ณ โอกาสนี้

ขอขอบคุณเจ้าหน้าที่ภาควิชาฟิสิกส์ คณะวิทยาศาสตร์ มหาวิทยาลัยนเรศวร ทุกท่านซึ่งอำนวยความสะดวกเกี่ยวกับอุปกรณ์เครื่องมือต่างๆ

ขอขอบคุณ Science Lab Center คณะวิทยาศาสตร์ มหาวิทยาลัยนเรศวร ที่สนับสนุนเครื่องมือและอุปกรณ์ในการทำวิจัย

ผศ.ดร.ธีระชัย บงการณ์

**หัวข้อวิจัย** การเตรียมเซรามิก BNT-BKT-KNN ด้วยวิธีการเผาไหม้

**นักวิจัย** ผศ.ดร.ธีระชัย บงการณ์

## บทคัดย่อ

BNNKT-0.20/0.03 ถูกแคลไซน์ที่อุณหภูมิระหว่าง 600-850 องศาเซลเซียส 2 ชั่วโมง และซินเตอร์ที่อุณหภูมิ 900-1050 องศาเซลเซียส เป็นเวลา 2 ชั่วโมง โครงสร้างเฟสและโครงสร้างจุลภาคถูกวิเคราะห์โดยใช้เครื่องเอกซ์เรย์ (XRD) และ กล้องจุลทรรศน์อิเล็กตรอนแบบส่องกราด (SEM) พบว่าในทุกๆ ตัวอย่างมีโครงสร้างเฟสบริสุทธิ์ที่อุณหภูมิแคลไซน์ และซินเตอร์ 750 องศาเซลเซียส และ 1025 องศาเซลเซียส เป็นเวลา 2 ชั่วโมง ตามลำดับ จากการศึกษารูปแบบการเลี้ยวเบนของรังสีเอกซ์เซรามิกมีโครงสร้างร่วมกันของรอมโบฮีดรอลและเตตระโกนอล จากการศึกษาโครงสร้างจุลภาค พบว่าเมื่อเพิ่มอุณหภูมิซินเตอร์ เกรนมีขนาดเพิ่มขึ้นและมีการแน่นตัวของโครงสร้าง จากการคำนวณหาค่าความหนาแน่นตัวมีค่าเท่ากับ 5.64 g/cm$^3$ (มีค่าเทียบกับทฤษฎีเป็น 95.0%) และค่าความหดมีค่าเท่ากับ 16.4% ซึ่งพบในตัวอย่างที่ถูกซินเตอร์ที่อุณหภูมิ 1025 องศาเซลเซียส

# CHAPTER I

# INTRODUCTION

## Overview

As is well known, piezoelectric materials have wide applications in electronic and microelectric devices. The most widely used piezoelectric materials are $PbZrO_3$-$PbTiO_3$ (PZT) based ceramics. However, in the process of obtaining this material, it is necessary to maintain the atmosphere with enriched vapor of lead oxide (PbO), which is opposite to the needs of environmental protection because of the toxicity. Furthermore, many countries have restricted the use of lead oxide by drafting legislation. Consequently, it is necessary and urgent to search for lead-free piezoelectric ceramics with excellent piezoelectric properties [1].

$Bi_{0.5}Na_{0.5}TiO_3$ (abbreviate to BNT), discovered by Smolenskii et al. in 1960 [1, 2], is an $ABO_3$ type ferroelectric with a perovskite phase. BNT is considered to be a promising candidate for lead-free piezoelectric ceramics with a relatively large remnant polarization ($P_r$ = 38 $\mu C/cm^2$) and a high Curie temperature ($T_c$ = 320 °C) [3, 4]. However, pure BNT ceramics have a high coercive field ($E_c$ = 7.3 kV/mm), making the poling of the ceramics extremely difficult. In addition, pure BNT ceramic usually exhibits very poor piezoelectricity ($d_{33}$ = 58 pC/N). To decrease the coercive field and improve the piezoelectric properties, a number of solid solutions of BNT with $ABO_3$-type ferroelectrics or non-ferroelectrics, such as BNT-$BaTiO_3$ [5], BNT-$NaNbO_3$ [6], BNT-$CaTiO_3$ [7], BNT-$SrTiO_3$ [7], BNT-$Bi_{0.5}K_{0.5}TiO_3$ [1] have been studied extensively. Xinyou et al. [5] reported that the dielectric constant ($\varepsilon_r$), the loss tangent ($\tan\delta$) and the piezoelectric constant ($d_{33}$) of 0.94 BNT-0.06 $BaTiO_3$ ceramics are 1650, 0.048 and 120 pC/N. In the case of 0.98 BNT-0.02 $CaTiO_3$, 0.80 BNT-0.20 $SrTiO_3$ and 0.98 BNT-0.02 $NaNbO_3$, the $d_{33}$ values were 75 [7], 133 [7] and 88 pC/N [6]. 0.82 BNT-0.18 $Bi_{0.5}K_{0.5}TiO_3$ (BNT-BKT) ceramics demonstrated the $\varepsilon_r$, $\tan\delta$, $d_{33}$, $k_p$ and $E_c$ of 893, 0.037, 144 pC/N, 29.0 % and 4 kV/mm [1]. Among these compositions, BNT-BKT ceramics have exhibited

excellent piezoelectric properties, but are still far from satisfactory in terms of practical applications.

The ternary system has demonstrated that a favorable design can improve piezoelectric and ferroelectric properties [8, 9, 10, 11, 12, 13, 14, 15, 16, 17, 18, 19]. The ternary system of BNT-BKT with $(K_{0.5}Na_{0.5})NbO_3$ (KNN) [14], were intensively investigated. Among the solid solutions that have been developed so far, $(1\text{-}x\text{-}y)Bi_{0.5}Na_{0.5}TiO_3–xBi_{0.5}K_{0.5}TiO_3–y(Na_{0.5}K_{0.5})NbO_3$ (BNKNT) and system has attracted considerable attention [10, 11, 12, 13, 14, 15, 16, 17, 18]. Singh et al. [14] revealed that the $0.79Bi_{0.5}Na_{0.5}TiO_3\text{-}0.20Bi_{0.5}K_{0.5}TiO_3\text{-}0.01K_{0.5}Na_{0.5}NbO_3$ ceramic has the largest strain ever reported for a polycrystalline lead-free ceramics (~0.80%), which is even higher than the strains obtained in Pb-based antiferroelectrics.

BNKNT have been prepared by the solid state reaction method, at a calcination stage above 900 °C and a sintering stage above 1150 °C for 3-5 h [14, 15, 18]. Although the solid-state reaction method is relatively simple, it is time consuming, energy intensive and a poor quality ceramic is obtained. Recently, our previous works have successfully fabricated high quality different oxides ceramics such as: $(Ba_{1-x}Sr_x)(Zr_xTi_{1-x})O_3$ [20], $Ba(Ti_{1-x}Zr_x)O_3$ [21], $(Pb_{1-x}Ba_xTiO_3)$ [22], $BaZrO_3$ [23] using the combustion technique. The advantages of this technique include inexpensive precursors, simple preparation process, and resulting good electrical properties with lower firing temperatures and a shorter dwell time [24, 25, 26]. Furthermore, from a survey of the literature, BNKNT ceramics, prepared by the combustion method, have not been studied. So, in this work, $(1\text{-}x\text{-}y)Bi_{0.5}Na_{0.5}TiO_3–xBi_{0.5}K_{0.5}TiO_3–yK_{0.5}Na_{0.5}NbO_3$ ($x$=0.20 and $y$=0.03) (abbreviated as BNNKT 0.20/0.03) powders and ceramics were prepared by the combustion method. The optimum firing temperatures on microstructure and phase transformation were also studied.

**Objectives of this research**

The objectives of this research are as follow:

1. To prepare $0.77Bi_{0.5}Na_{0.5}TiO_3–0.02Bi_{0.5}K_{0.5}TiO_3–0.03(Na_{0.5}K_{0.5})NbO_3$ , BNNKT-0.20/0.03 ceramics ternary system using the combustion technique.

2. To investigated the optimum calcination and sintering conditions of $0.77Bi_{0.5}Na_{0.5}TiO_3–0.02Bi_{0.5}K_{0.5}TiO_3–0.03(Na_{0.5}K_{0.5})NbO_3$ , BNNKT-0.20/0.03 ceramics for combustion preparation.

3. To study the effect of calcination and sintering temperatures on the crystal structure, microstructure, electrical properties of $0.77Bi_{0.5}Na_{0.5}TiO_3–0.02Bi_{0.5}K_{0.5}TiO_3–0.03(Na_{0.5}K_{0.5})NbO_3$ , BNNKT-0.20/0.03 ceramics prepared via the combustion technique.

# CHAPTER II

# THEORY AND LITERATURE

## Perovskite Structure

Since the ferroelectric properties of barium titanate were reported by Von Hippel in 1945, $ABO_3$ compound with the perovskite structure have been studied extensively [27, 28]. These studies have resulted in the discovery of many new ferroelectric and piezoelectric materials. Most of the literatures on perovskite-type compounds have concentrated on these properties.

Perovskite is the name of the mineral calcium titanate ($CaTiO_3$). Most of the useful piezoelectric (ferroelectric) ceramics, such as bismuth sodium titanate ($Bi_xNa_{1-x}TiO_3$), barium titanate ($BaTiO_3$), lead titanate ($PbTiO_3$), lead zirconate titanate ($PbZr_{1-x}Ti_xO_3$), lead lanthanum zirconate titanate (PLZT), potassium niobate ($KNbO_3$), potassium sodium niobate ($KNa_xNb_{1-x}O_3$), have a perovskite structure. These oxide ceramics have the general chemical formula $ABO_3$, where O is oxygen in the centers of the faces. Arepresents a cation with a larger ionic radius on the corners, and Brepresents a cation with smaller ionic radios in the center of the body [29, 30, 31]. Figure 1 shows a cubic $ABO_3$perovskite-type unit cell and three–dimensional network of $BO_6$- octrahedral. A sites are occupied by $Bi^{2+}$, $Ba^{2+}$,$Pb^{2+}$, $K^+$or $Na^+$ions, and B sites by $Ti^{4+}$, $Zr^{4+}$, $Nb^{5+}$or $Ta^{5+}$ions.

Binary or ternary solid solutions of more than one of these simple perovskites allows for the creation of more complex perovskites. Essentially, multiple elements split the occupancy of the A or B site and must average out to the appropriate charge for that site according to the same principles used in the case of the three simple perovskite types listed above. The high stability of the perovskite structure allows for highly complex charged compensated compositions to form. The general formula for complex perovskites can be written as $(A'A'')^{XII}(B'B'')^{VI}X_3$. While many of the complex perovskite families are known to be relax or ferroelectric, there has been significant success in modifying ferroelectric compositions such as $(Bi_{0.53}{}^{3+}K_{0.5}{}^{1+})Ti0_3$, $(Bi_{0.5}{}^{3+}Na_{0.5}{}^{1+})Ti0_3$, and many combinations of these two. Another highly investigated

system to be covered is $(K_{0.5}^{1+}Na^{1+})(Nb_x^{5+}Ta_{1-x}^{5+})O_3$, with even further elements being introduced to enhance the piezoelectric properties.

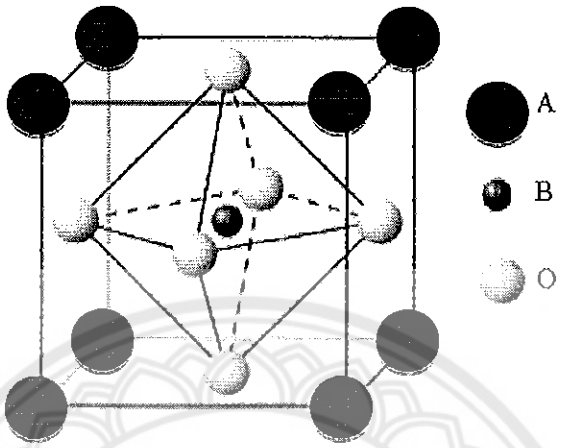


**Figure 1 The perovskite structure as an $ABO_3$perovskite-type unit cell [27]**

**Piezoelectricity**

Piezoelectricity was discovered in 1880 by Jacques and Pierre Curie during their systematic study of the effect of pressure on the generation of aelectrical charge by crystals such as quartz, zincblend, and tourmaline [29, 30, 32]. The name "piezo" is derived from the Greek, meaning "to press", hence piezoelectricity is the generation of electricity as a result of mechanical pressure. Many piezoelectric materials are not ferroelectric but all ferroelectrics are piezoelectric. Two effects are operative in piezoelectricity. The direct effect is identified with the phenomenon whereby an electrical charge (polarization) is generated from mechanical stress, whereas the converse effect is associated with the mechanical movement generated by the application of an electrical field. Both of these effects are illustrated in Figure 2

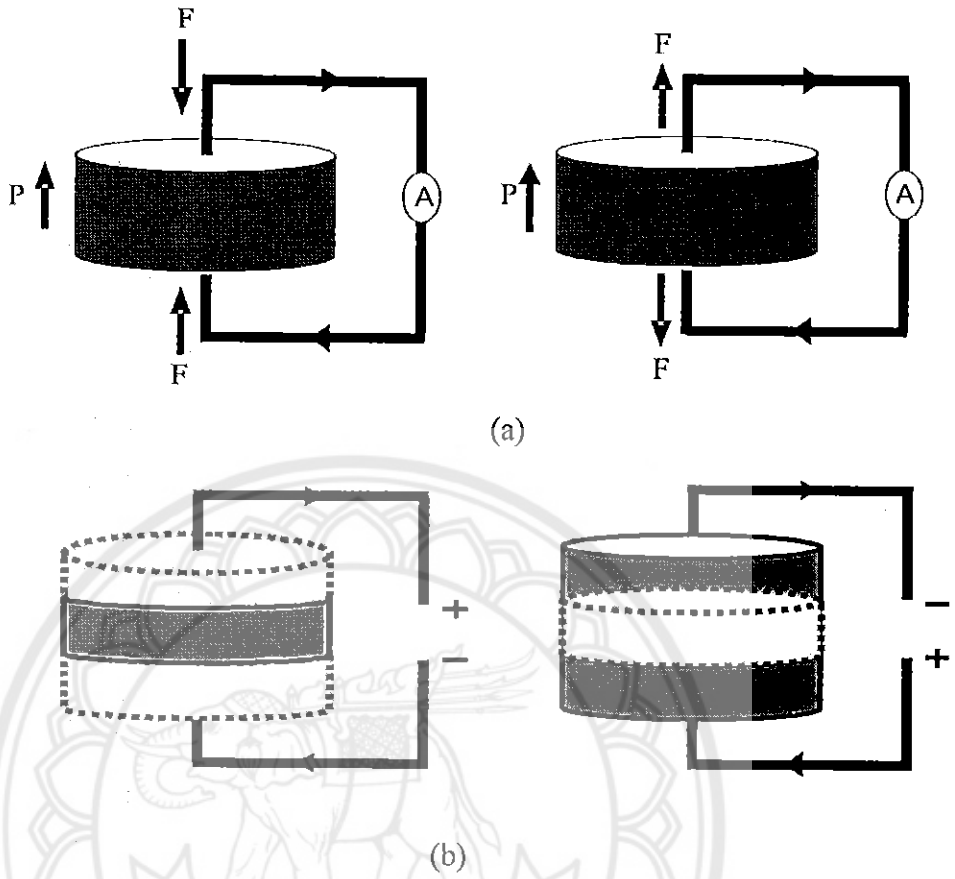


**Figure 2 Piezoelectric effects in ferroelectric ceramics**
**(a) direct effect (b) converse effect [29]**

The basic equations that describe these two effects in regard to electric and elastic properties are

$$D = dT + \varepsilon^T E \quad (1)$$

$$S = s^E T + dE \quad (2)$$

Where D is the dielectric displacement (consider it equal to polarization), T the stress, E the electric field, S the strain, d a piezoelectric coefficient, s the material compliance (inverse of modulus of elasticity), and ε the dielectric constant(permittivity). The subscripts indicate a quantity held constant: in the case of $\varepsilon^T$, the stress is held constant, which means that the piezoelectric element is

mechanically unconstrained, and, in the case of $s^E$, the electric field is held constant, which means the electrodes on the element are shorted together.

**Ferroelectrics**

Ferroelectricity is a phenomenon which was discovered by Valasek in 1921 [33]. It has become customary to call ferroelectricity the phenomenon exhibited by these crystals and ferroelectric the crystal themselves. This is due to a formal similarity of the ferroelectric phenomenon with that of ferromagnetism. The similarity is mainly phenomenological. As ferromagnetic materials exhibit a spontaneous magnetization and hysteresis effects in the relationship between magnetization and magnetic field, ferroelectric crystals show a spontaneous electric polarization and hysteresis effects in the relation between the dielectric displacement and the electric field. This behavior is mostly observed in certain temperature regions below by transition temperature (Curie temperature) where those crystals above are this transition temperature are no longer ferroelectric.

The crystal symmetries of the paraelectric and ferroelectric phase are an important factor in displaying the ferroelectric behavior of the materials. The lattice structure described by the Bravais unit cell of the crystal governs the crystal symmetry. Though there are thousands of crystals in nature, they all can be grouped together into 230 microscopic symmetry types or space groups based on symmetry elements. It can be shown by the inspection of the 230 space groups that there are just 32 point groups. As shown in Figure 3, the 32 point groups can be further classified into (a) crystal having a center of symmetry and (b) crystals which do not possess a center of symmetry (noncentrosymmetric). There are 21 classes of noncentrosymmetric, a necessary condition for piezoelectricity to exist, and only 20 are piezoelectric. Among these 20 point groups, only 10 can display a spontaneous polarization, which is designated as pyroelectric. A subgroup of the spontaneous polarized pyroelectric is a category of materials known as ferroelectrics. Ferroelectrics are a special class of materials in which a permanent electric dipole can be reoriented between equilibrium states by the external electric field. Continuing Valasek's analogy between ferroelectric and ferromagnetic, the dependence of the polarization on an applied electric field can be seen by polarization versus electric field i.e. (P-E)

hysteresis loop as shown in Figure 4. The hysteresis loop is typically observed using the simple circuit described by Sawyer-Tower [35]. One parameters obtained from the hysteresis loop measurement, the remnant polarization ($P_r$) is the crystal spontaneous polarizes along one of the allowed direction without applied electric field. The field required to reverse the polarization is known as the coercive field ($E_c$). Ferroelectric materials are divided into two main categories as normal and relaxor ferroelectrics.

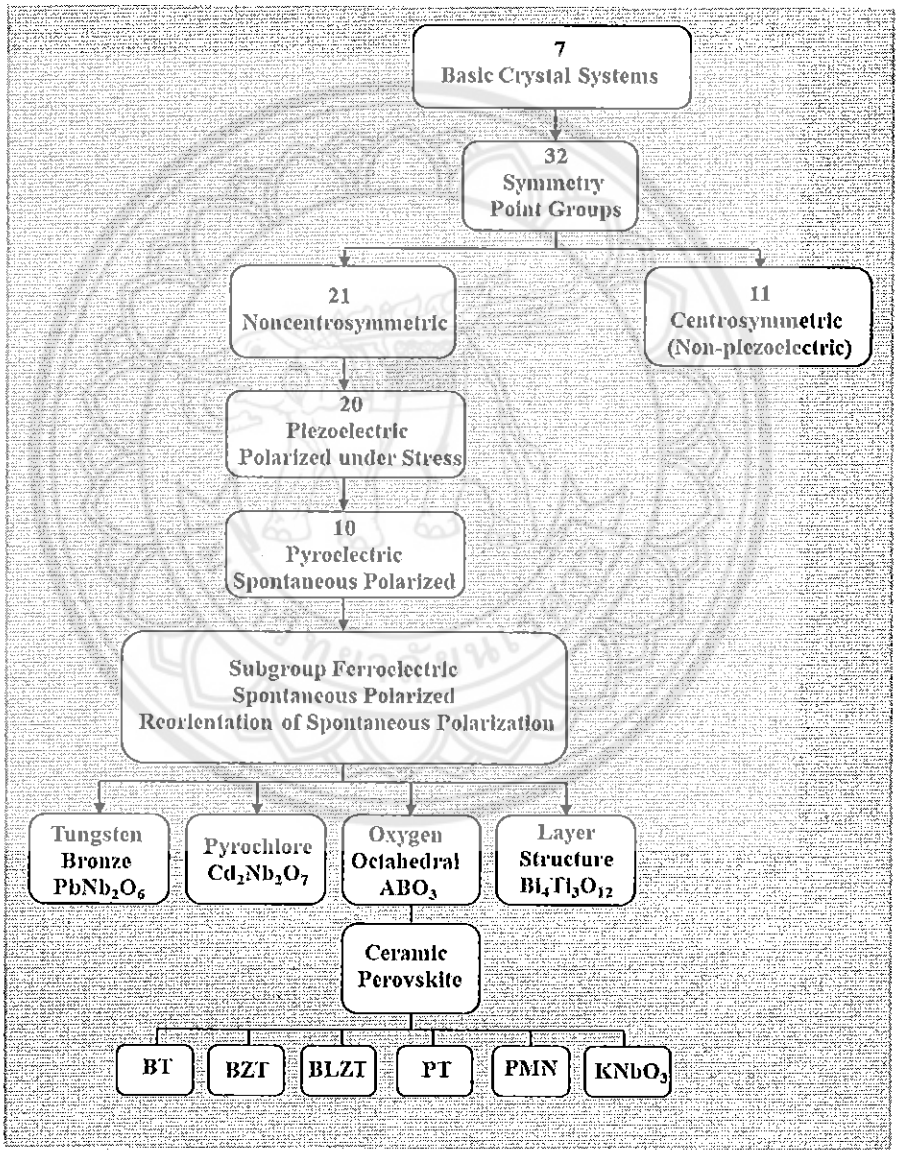


**Figure 3 Interrelationship of piezoelectric and subgroups on the basis of symmetry [33]**

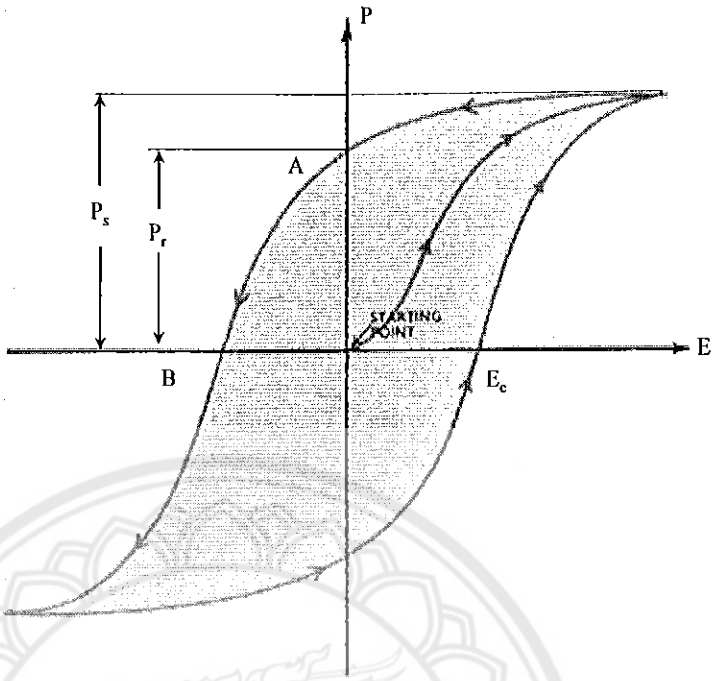


**Figure4 A ferroelectric hysteresis loop [33]**

**Normal ferroelectric**

Normal ferroelectric materials have a sharp phase transition which occurs at a specific temperature called the Curie temperature, $T_c$. The $T_c$ is the temperature which the crystal structure transforms from the paraelectric state into the ferroelectric state and vice versa [36, 37, 38, 39]. In the paraelectric state, the dielectric permittivity obeys the Curie-Weiss law:

$$\varepsilon_r = \frac{C}{T - T_0} \tag{3}$$

Where C is the Curie-Weiss constant, T is the temperature and, $T_0$ is the Curie-Weiss temperature. The Curie temperature ($T_c$) and the Curie-Weiss temperature ($T_0$) should not be confused. The Curie temperature is the actual transformation temperature, but the Curie-Weiss temperature is found by extrapolating the plot of the Curie-Weiss law, as shown in Figure 5. The Curie temperature and Curie-Weiss temperature typically differ by only a small amount that depends on the type of phase formation the material undergoes. The Curie-Weiss temperature

can be as much as ten degrees lower than the Curie temperature for first-order phase transformations and the two can be nearly equal for second-order phase transformations (first order phase transformations are those in which the first derivative of the free energy, with respect to temperature, is discontinuous; second order phase transitions are those in which the second derivative is discontinuous)

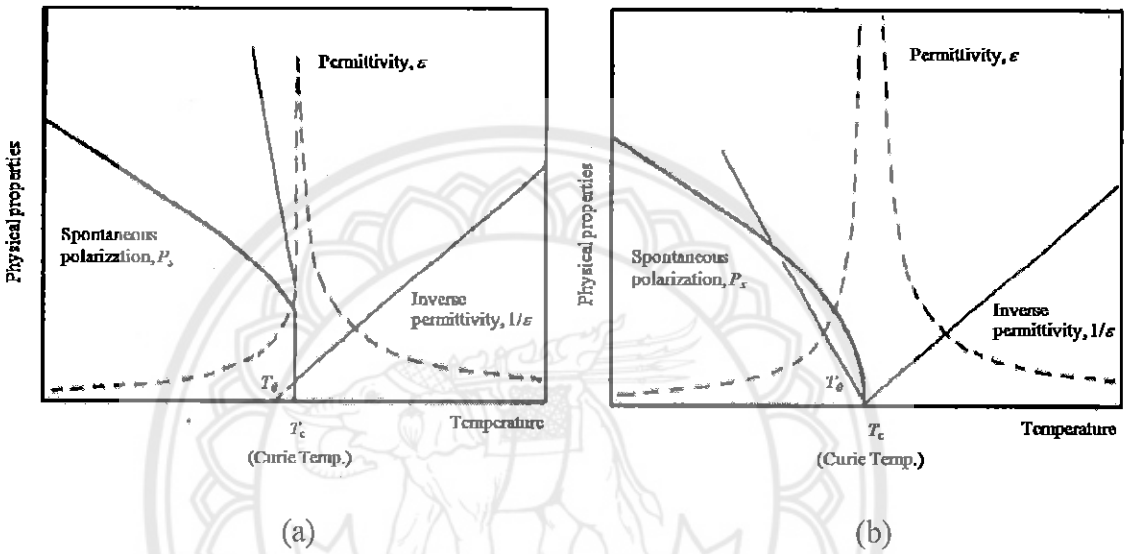


**Figure 5 Phase transition in a ferroelectric (a) first order and (b) second order [36]**

**Relaxor ferroelectric**

The relaxor behaviorswere recognized by Cross [40]. Relaxor could be classified into two states: non-ergodic and ergodic [41]. Non-ergodic one can be transforms irreversibly into the ferroelectric state and ergodic does reversibly. Several material properties distinguish normal and relaxor ferroelectrics are summarized in Table 1 and below:

(i) The sharp well-defined phase transition temperature (Curie temperature) found for normal ferroelectrics is absent for relaxors. The dielectric constant maximum does not distinguish the exact paraelectric to ferroelectric phase transition as in normal ferroelectrics. The paraelectric to ferroelectric phase transition becomes broad and diffuse in relaxor and Curie ranges replace the Curie temperature. The permittivity of a relaxor is also dispersive in nature at radio frequencies, where

the permittivity decreases and the temperature of the dielectric constant maximum ($T_m$) shifts to higher temperature with increasing frequency.

(ii) In relaxor ferroelectrics, the dielectric constant does not follow Curie-Weiss law behavior above the ferroelectric transition. Instead, relaxers follow Curie-Weiss square law (sometimes called the quadratic Curie-Weiss law):

$$\frac{1}{\varepsilon_r} - \frac{1}{\varepsilon_m} = \frac{(T-T_m)^2}{C'} \tag{2.4}$$

where $\varepsilon_r$ is the relative dielectric constant, $\varepsilon_m$ is the dielectric constant maximum, $T_c$ is the temperature of the dielectric constant maximum and $C'$ is the modified Curie-Weiss constant. This quadratic relation is valid for materials that display diffuse phase transitions. Most materials; however, show intermediate behavior between the linear and quadratic limits. Uchino et al. proposed a variation power law as the modified Curie-Weiss law [41]

$$\frac{1}{\varepsilon_r} - \frac{1}{\varepsilon_m} = \frac{(T-T_m)^\gamma}{C'} \tag{4}$$

where $\gamma$ is the critical exponent. The value of the critical exponent can vary from $\gamma = 1$, for purely normal ferroelectrics, to $\gamma = 2$, for purely relaxor ferroelectrics. The qualitative method to determine the parameter of relaxor ferroelectric is by plotting the inverse dielectric constant as a function of temperature as a log-log scale.

(iii) Another feature which distinguishes normal and relaxor ferroelectrics is the behavior of polarization. The relatively rapid decrease of the polarization to zero is found in normal ferroelectrics at $T_c$. This gradual decrease extends to temperature above $T_m$ before reaching zero. This can be observed in P-E hysteresis loops. At temperatures well below $T_m$, relaxors show a typical P-E hysteresis loop; however, the loops decay slowly into simple non-linearity as the temperature increases through the Curie range.

(iv) Asthe temperature decreases, the number of polar region increases so that the regions are in contact; however, since these regions are oriented along different

polarization directions the crystal still appears isotropic. Several characteristics are caused by the polar regions orienting along difference axes. First, relaxor ferroelectrics exhibit weak remnant polarization. Second, due to the long coherence length of XRD, relaxor ferroelectrics appear cubic since they do not exhibit x-ray peak splitting. Third, under optical microscopy, relaxor ferroelectrics exhibit negligible birefringence [42].

**Antiferroelectric**

An antiferroelectric crystal is defined as a crystal whose structure can be considered as being composed of two sublattices polarized spontaneously in antiparallel directions and in which a ferroelectric phase can be induced by applying an electric field. Experimentally, the reversal of the spontaneous polarization in ferroelectrics is observed as a single hysteresis loop, and the induced phase transition in antiferroelectrics as a double hysteresis loop (Figure 6), when a low-frequency ac field of a suitable strength is applied [43].

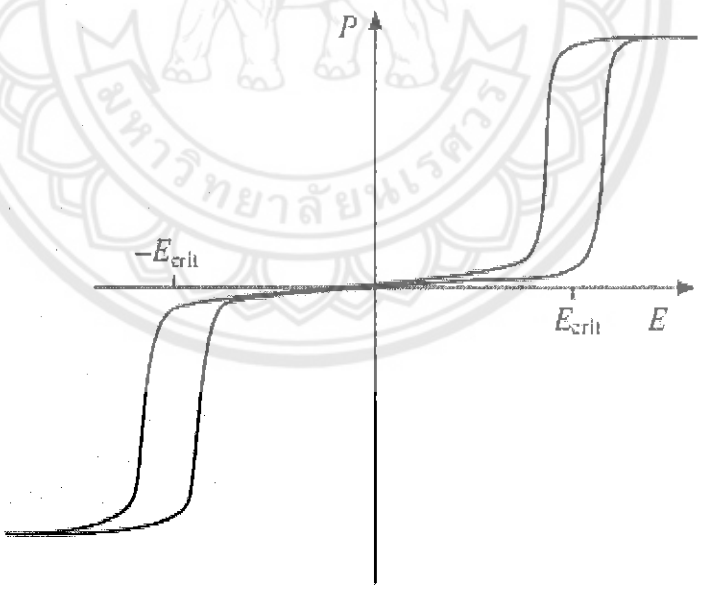


**Figure 6 Antiferroelectric hysteresis loop [43]**

**Table 1 Differentproperty of normal and relaxor ferroelectrics [36]**

| Properties | Normal ferroelectrics | Relaxor ferroelectrics |
|---|---|---|
| Permittivity temperature dependence $\varepsilon_r = \varepsilon_r(T)$ | Sharp 1st or 2nd order phase transition at Curie temperature ($T_c$) | Broad-diffuse phase transition around Curie maximum ($T_m$) |
| Permittivity temperature and frequencydependence $\varepsilon_r = \varepsilon_r(T, \omega)$ | Weak frequency dependence | Strong frequency dependence |
| Permittivity behavior in paraelectric range ($>T_c$) | Follow Curie-Weiss law $\varepsilon_r = C/(T = T_0)$ | Follow Curie-Weiss square law $1/\varepsilon_r = 1/\varepsilon_m + (T-T_m)^2 /2\varepsilon_m\delta^2$ |
| Remnant polarization | Strong remnant polarization | Weak remnant polarization |
| Scattering of light | Strong anisotropy (birefringent) | Very weak anisotropy to light (pseudo-cubic) |
| Diffraction of X-ray | Line splitting owing to spontaneous deformation from paraelectric to ferroelectric phase | No X-ray line slitting giving a pseudo-cubic structure |

**Paraelectric**

Paraelectricity is the ability of many materials (specifically ceramic crystals) to become polarized under an applied electric field. Unlike Ferroelectricity; this can happen even if there is no permanent electric dipole that exists in the material, and removal of the fields results in the polarization in the material returning to zero, as shown in Figure 7. The mechanisms which give rise to paraelectric behavior are the distortion of individual ions (displacement of the electron cloud from the nucleus) and the polarization of molecules or combinations of ions or defects. Paraelectricity

occurs in crystal phases in which electric dipoles are unaligned (i.e. unordered domains that are electrically charged) and thus have the potential to align in an external electric field and strengthen it. In comparison to the ferroelectric phase, the domains are unordered and the internal field is weak. The $LiNbO_3$ crystal is ferroelectric below 1430 K, and above this temperature it turns to paraelectric phase. Other perovskites similarly exhibit paraelectricity at high temperatures [44].

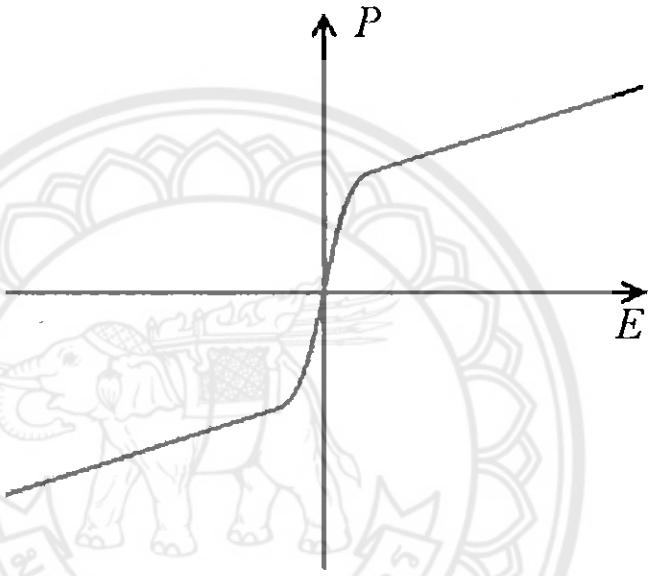


**Figure 7 Paraelectric hysteresis loop [44]**

**Morphotropic Phase Boundary (MPB)**

An MPB can be located at the compositional boundary between two perovskite materials with different symmetries by controlling the ratio of each perovskite component. The most common example of this phenomenon is the solid solution of lead zirconate-titanate, or $Pb(Zr_xT_{1-x})O_3$ (PZT). In fact, PZT is the most analyzed system with an MPB due to its exceptionally large and constant piezoelectric properties. This is due to the fact that PZT shows a nearly vertical, temperature independent, phase boundary between the $PbTiO_3$ (tetragonal) and $PbZrO_3$ (rhombohedral) phases at a composition of x~0.52, as shown in Figure 8 [45]. The origin for this maximization of the piezoelectric response in this MPB region is generally explained by the high degree of freedom for the electric dipoles.

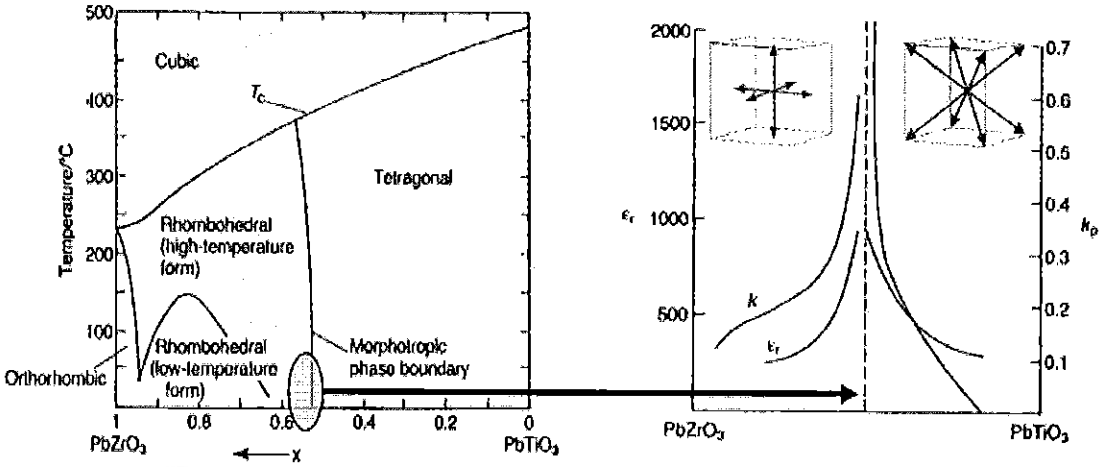


**Figure 8 Phase diagram and piezoelectric properties for $Pb(Zr_xTi_{1-x})O_3$ceramic [45]**

This allows them to be easily oriented via an electric field in a large number of directions, essentially combining the possible orientations of tetragonal (6 along [001]) with those of rhombohedral systems (8 along [111]). Domain systems arising can orient along all of these directions and form a more highly oriented polycrystalline sample under optimal poling. More recent structural studies also indicate another possibility, that an intermediate phase of monoclinic symmetry may exist at the MPB composition and results in the enhancement of piezoelectric and dielectric properties [46]. Although many lead free systems are described as having an MPB, usually the phase transition observed is not highly independent of temperature, with fairly wide ranges of compositions and the resulting enhancement of properties is not as compelling. These transitions are more aptly described by the term polymorphic phase transition.

## Typical methods to synthesize ceramics

### Solid-state reaction method

Solid-state reaction method is the most widely used method for the preparation of polycrystallinesolids from a mixture of solid starting materials. This method involves chemical decomposition, where solid reactants are heated to produce a new solid and normally use simple oxides powders such as carbonates, hydroxides, nitrates, sulfates, acetates, oxalates, alkoxides and other metal salts for

preparation. The solids do not react together at room temperature over normal time scales and it is necessary to heat them to much higher temperatures, often to 1000 to 1500 °C in order for the reaction to occur at an appreciable rate.An example of reaction between barium carbonate and titanium oxide at high temperature produce barium titanate by using solid-state reaction method.

$$BaCO_3(s)+TiO_2(s)\text{-- (}\sim 1200\ ^\circ C)\text{----->}BaTiO_3(s)+CO_2(g) \quad (5)$$

Solid-state reactions generally have an advantage in terms of production cost. However, it is commonly understood that the conventional solid state method requires compulsory grinding of different oxide mixtures for long periods of time as well as sintering. In addition, the synthesized component distributions are not homogeneous and particle sizes are relatively large [47, 48].

**Sol-gel processing**

Sol-gel process is a method for producing solid materials from small moleculesin a solution (sols) agglomerate and under controlled conditions eventually link together to form a coherent network (gel). The method is used for many applications in synthesis of novel materials. The advantages of the sol-gel process in general are high purity, homogeneity and low temperature. For a lower temperature process, there is a reduced loss of volatile components are thus the process is more environmental friendly. In addition, some materials that cannot be made by conventional means because of thermal and thermodynamically instability can be made by this process. However, the disadvantages are also real. The starting materials can be fairly expensive [49, 50].

**Co-precipitation method**

Co-precipitation (CPT) is the carrying down by a precipitate of substances normally soluble under the conditions employed. This method proceeds in two stages. First stage, the impurity is trapped either on the surface or inside the growing particles. If the growing particles have a crystal structure, then the impurity will become localized at regions of the solid phase with a perfect structure. During rapid precipitation, the growing particles will trap non-equilibrium impurities, which are usually in homogeneously distributed through the volume of the solid phase.

In the second stage, the concentration of defects within the precipitate decrease and the particles are flocculated. Impurities trapped during the first stage return either partially or completely to the medium. The concentration of impurities in the solid phase becomes equalized. The crystals acquire an equilibrium composition that depends only on the composition and temperature of medium [49, 50].

**Hydrothermal synthesis method**

Hydrothermal synthesis is generally defined as crystal synthesis or crystal growth under high temperature and high pressure water conditions from substances which are insoluble in ordinary temperature and pressure (<100 °C, <1 atm). Advantages of the hydrothermal synthesis method include the ability to synthesis crystals of substances which are unstable near the melting point, and the ability to synthesis large crystals of high quality. Disadvantages are the high cost of equipment and the inability to monitor crystals in the process of their growth. Hydrothermal synthesis can be affected both under temperatures and pressures below the critical point for a specific solvent above which differences between liquid and vapour disappear, and under supercritical conditions. The solubility of many oxides in hydrothermal solutions of salts is much higher than in pure water; such salts are called mineralizers. There is also a group of solvothermal synthesis methods, relational to hydrothermal methods; this group of methods is based on the use of organic solvents and supercritical $CO_2$.

**Combustion technique**

Combustion techniqueuses the energy released from the oxidation-reduction reaction. It has emerged as an important technique for the synthesis and processing of advanced ceramics, which involves a self-sustained reaction between reaction materials and fuel (e.g., urea, glycine, citric acid, alanine or carbohydrazide). The advantages of this technique include inexpensive precursors, simple preparation process, and resulting good electrical properties with lower firing temperature and shorter dwell time [24, 25, 26].

**I. Types of organic compounds**

Hwang et al. [52] has investigated decomposition of the five fuels by Thermogravimetric analysis. They choose the fuel such as glycine, urea, alanine, citric acid or carbohydrazide. Some properties of five fuelsthey select are shown in Table

2.The results of the thermal analysis show that there were different weight losses of organic fuels. When using carbohydrazide as organic fuel, indicating that the chemical reaction took place very rapidly. But remaining weight is 22% of its original weight. While using glycine and alanine as organic fuels, the thermogravimetric of both demonstrated similar results. Their reactions are very fast and remaining weight lower than 10%. When using urea and citric acid as organic fuels, the chemical reaction was not rigorous when compared with glycine and alanine.

**II. Influence of fuels and development of novel synthesized combustion technique of powders and ceramics**

The crystal structure and microstructure of Ni-Zn ferrites prepared by combustion technique with various organic fuels was studies by Hwang et al. [52]. They result show that the pure phase of Ni-Zn was obtained while using glycine, alanine and corbohydrazide. While using urea and citric as organic fuels, the impurities phase was obtained existed in the diffraction pattern, as seen in Figure 10. The nanocrystalline sizes are ranging between 20.2 and 43.7 nm, as seen in Table 3. The results indicated that the ceramic synthesized by the combustion technique produced nanocrystalline sizes.

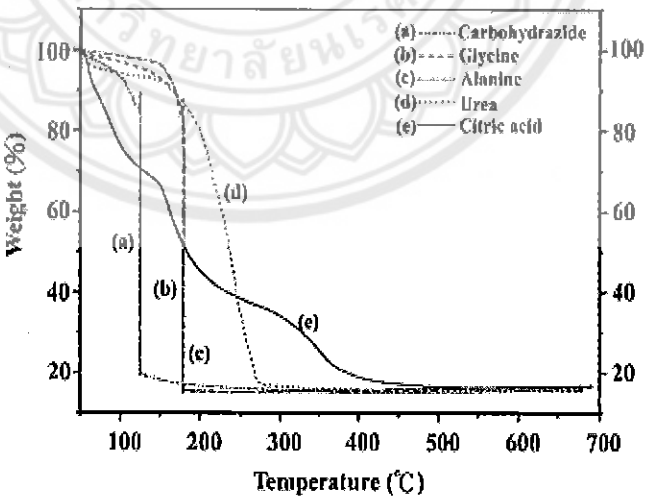


**Figure 9 Thermogravimetric of fuel [52]**

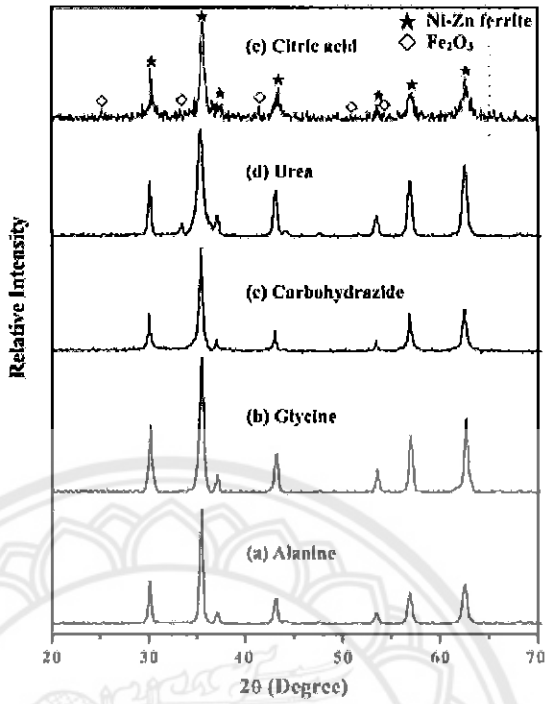


**Figure 10 XRD patterns of the Ni-Zn ferrites with various organic fuels: (a) alanine (b) glycine (c) carbohydrazide (d) urea and (d) citric acid [52]**

Our group successfully fabricated ceramics oxide by the combustion technique such as $Pb_{1-x}Ba_xTiO_3$(PBT), $(Ba_{0.25}Sr_{0.75})(Zr_{0.75}Ti_{0.25})O_3$ (BSZT)etc. [20, 22]. In the case of PBT, the result show that the combustion technique produced nano-powders of PBT powders, with average size around 54-77 nm, as seen in Figure 11. A high density above 96.5% with calcined between 1,000 and 1150 °C and sintered between 1200 and 1250 °C for only 2 h can be prepared by the combustion technique, which shorter time than prepared by the solid state reaction method. In the case of $(Ba_{0.25}Sr_{0.75})(Zr_{0.75}Ti_{0.25})O_3$, it was synthesized using combustion technique compared with solid state reaction method. The results shown that the particle size of BSZT powder prepared via the combustion technique is 0.13-0.30 μm and the solid state reaction method is 0.18-0.38 μm. Moreover, the result shows that the combustion technique has potential to reduce the calcination temperature and is suitable for prepared oxide ceramic. Therefore, the combustion method was chosen for preparation BNKFT, BNKNT and BNKLT ceramics in this work.

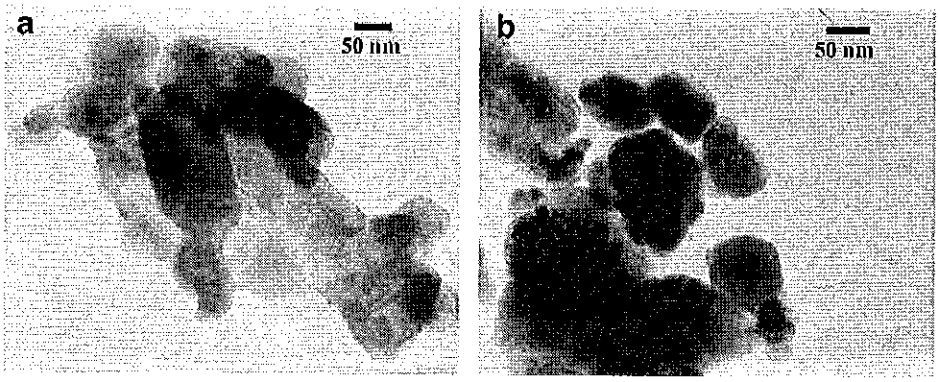


**Figure 11** TEM micrographs of (a) original magnification x120,000 of $Pb_{0.60}Ba_{0.40}TiO_3$ powder calcined at 1050 °C and (b) original magnification x100,000 of $Pb_{0.20}Ba_{0.80}TiO_3$ powder calcined at 1150 °C [20]

**Table 2** Someproperties of organic compounds [52]

| Properties | Organic component | | | | |
|---|---|---|---|---|---|
| | Alanine | Glycine | Carbohydrazide | Urea | Citric acid |
| Structure formula | 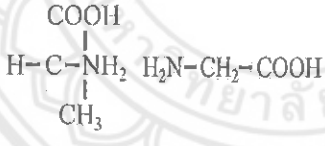 |  | 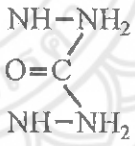 | 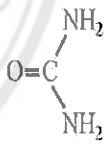 | 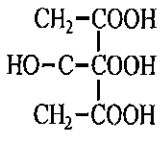 |
| Molecular weight (g/mol) | 80.1 | 90.1 | 75.1 | 60.1 | 192.1 |
| Heat of combustion (kJ/g) | 18.2 | 13.0 | 12.6 | 10.5 | 10.2 |
| Decomposition temperature (°C) | 314 | 262 | 153 | 135 | 175 |

**Table 3 Effect of various fuels of the Ni-Zn ferrites prepared by the combustion technique [52]**

| Fuel | $T_m$[a] (°C) | Amount of gas produced (mole) | Crystallite size[b] (nm) | Surface area ($m^2/g$) | Carbon content (wt.%) | $Ni^{2+}$ :$Zn^{2+}$ : $Fe^{3+}$ | $M_s$[c] ($Am^2/kg$) |
|---|---|---|---|---|---|---|---|
| Alanine | 1245 | 20.7 | 38.6 | 24.7 | 1.64 | 0.500:0.467: 1.920 | 60.8 |
| Glycine | 1150 | 26.2 | 32.7 | 31/2 | 1.53 | 0.500:0.471: 1.922 | 62.4 |
| Carbohydrazide | 1380 | 24.0 | 43.7 | 20.6 | 1.87 | 0.500:0.462: 1.917 | 58.5 |
| Urea | 785 | 30.7 | 20.2 | 48.5 | 3.82 | 0.500:0.483: 1.936 | 57.2 |
| Citric acid | 725 | 26.2 | 22.7 | 44.1 | 5.75 | 0.500:0.490: 1.947 | 55.8 |

**Note:** [a]$T_m$ the maximum combustion temperature, measured by Pt-Pt-Rh thermocouple.

[b] Crystalline size of the as-synthesized Ni-Zn ferrite powders calculated from the line broadening of the (311) XRD peak by Sherrer formula.

[c]$M_s$ the saturation magnetization of the sintered Ni-Zn ferrite samples (950 °C/2h).

**One Component Systems**

Useful lead-free materials are often binary or ternary solid solutions. Before discussing these more complex material systems in next section, this section introduces and discusses the member compositions of based ceramics.

**$(Bi_{0.5}Na_{0.5})TiO_3$ (BNT)**

Since BNT was discovered by Smolenskii et al. in 1960 [2, 53], it has gained a lot of attentions from various aspects. It has high Curie temperature ($T_c$=320°C). Recently, detailed studies on the structure transformation of BNT single crystals have been carried out by Hiruma et al. using x-ray diffraction. They found that the pure

BNT is a perovskite-structured ferroelectric with rhombohedral symmetry at room temperature (RT), and its phase transitions are complicated [54]. The phase transition temperatures $T_{R-T}$ from rhombohedral to tetragonal and $T_{T-C}$ from tetragonal to cubic are approximately 230 and 320°C upon heating, respectively, for BNT single crystals. Lee et al. [55] studies the lattice parameter of BNT ceramic system calculated by the Rietveld method with XRD patterns, and they reported that the lattice constants of BNT ceramics are a=3.888 Å.

Lencka et al. [56] studied the microstructure of BNT powder prepared by hydrothermal method, were investigated using field emission scanning microscopy (FESEM), x-ray diffraction (XRD) and specific surface areas were measured by multipoint BET technique. The average particle size calculated from FESEM range from 40 and 150 nm can be seen in Figure 12. Crystallite sizes calculated from the XRD peak broadening range from 13 to 28 nm. The measured specific surface areas range from 20.0 $m^2/g$ to 27.6 $m^2/g$.Saradhi et al. [57] investigated the grain size of BNT ceramics prepared by conventional double sintering method and analyzed by scanning electron microscope (SEM). They revealed that the average grain size ranged from 1 to 3 μm, corresponding to the result of Zuo et al. [50].

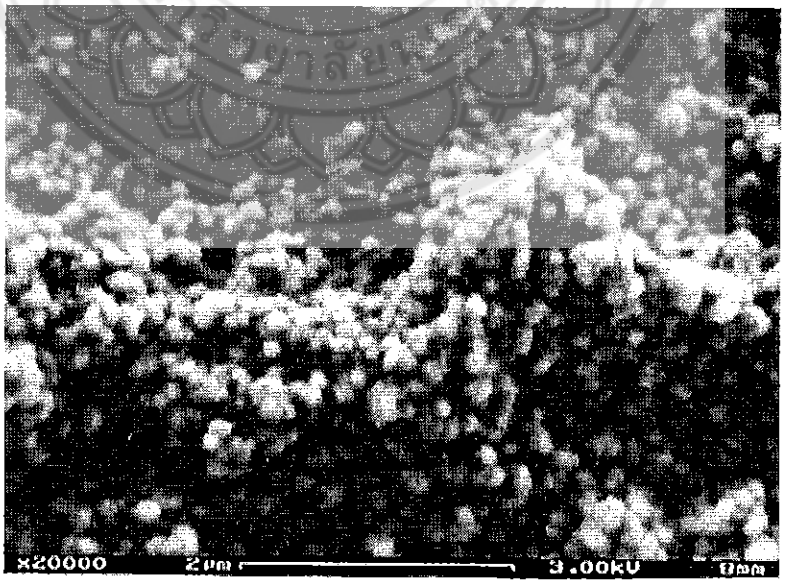


**Figure 12 FESEM micrograph of the BNT powders [57]**

The temperature dependences of the dielectric constant ($\varepsilon_s$) and the loss tangent (tanδ) from 20 Hz to 1 MHz of BNT ceramics between RT and 500 °C are shown in Figure 13. There are two dielectric peaks anomalies. The appearance of first temperature peak ($T_d$) is caused by the phase transition from rhombohedral ferroelectric to tetragonal anti-ferroelectric phase. The appearance of second temperature peak ($T_m$) can be explained by the transition from tetragonal anti-ferroelectric to cubic paraelectric phase $T_d$ and $T_m$ occurred in a temperature at 187 °C and 325 °C. The tan δcurves of the BNT reveal only one peak near the temperature of $T_d$ and tan δ sharply increases when temperature is higher than $T_m$ [54].

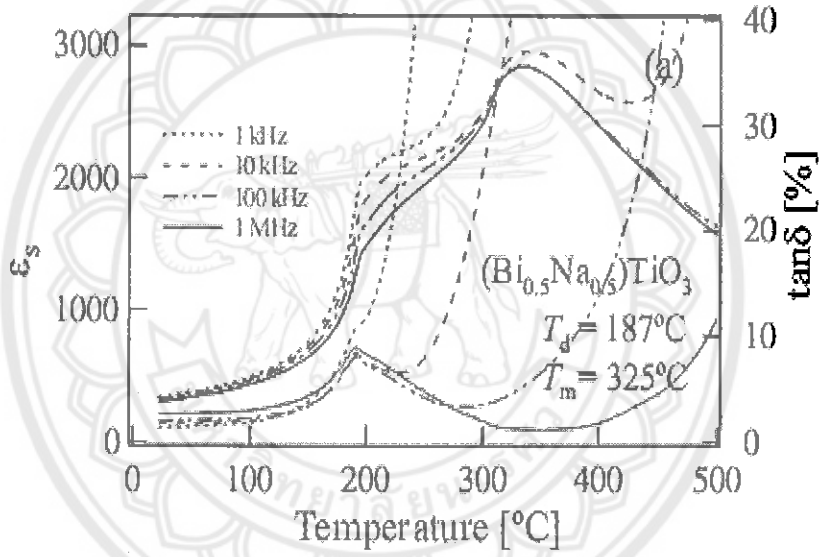


**Figure 13 Temperature dependences of dielectric constant ($\varepsilon_r$) and loss tangent (tanδ) in temperature range from RT to 500 °C of BNT ceramics [54]**

The BNT ceramics shows the strong ferroelectric property of a large remnant polarization and relatively high piezoelectric properties compared with other lead-free piezoelectric ceramics. Zuo et al. [58] reported that the remnant polarizations, piezoelectric constant and coupling factor of BNT are 38 $\mu C/cm^2$, 75 pC/N and 15.4 %. Nevertheless, the applications of BNT are limited by its high coercive field and its high conductivity. Coercive fields vary greatly between 2 kV/mm for sol-gel derived BNTand 7.3 kV/mm for BNT prepared by a mixed oxide route [59]. To solve

these problems and improve the electric properties, various types of compounds were added into BNT to form solid solution, such as $BaTiO_3$, $SrTiO_3$, $CaTiO_3$, $Bi_{0.5}K_{0.5}TiO_3$, $NaNbO_3$, $Ba(Cu_{0.5}W_{0.5})O_3$, and discussing complex material in next section.

**$(Bi_{0.5}K_{0.5})TiO_3$ (BKT)**

BKT was first determined to be ferroelectric by Smolenskii et al. [60], which was found in 1961 at the same time as BNT. Its unit cell is similar is that if BNT but with all the sodium ions replaced by potassium ions. It is a tetragonal ferroelectricperovskite at room temperature and a relatively high Curie temperature $T_c$ of 380 °C. Above the Curie temperature BKT is cubic paraelectric [61]. Ivanova et al. [62], reported the lattice parameter of BKT as a = 0.3913 nm, c = 0.3990 nm at room temperature.

SEM micrograph of BKT powder was studied by Hou et al. [63], and they reported that the particles size was very small and relatively uniform, as can be seen in Figure 14. The average particle size was between 100 and 200 nm. FESEM micrograph of the BKT powders demonstrated a uniform spherical particle with the diameter ranges from 40 to 150 nm, which was studies by Lencka et al. [56], as shown in Figure 15.

The dielectric constant ($\varepsilon_r$) and dielectric loss ($\tan\delta$) of BKT ceramics were studied by Hiruma et al. [64]. The $\varepsilon_r$ and $\tan\delta$ at room temperature of BKT are 524 and 6.8% at 1MHz. Some authors showed the values of room temperature dielectric constant $\varepsilon_r$ and loss tan δ at 1 kHz are 733 and 4.8 %. Yang et al. [65] studies the dielectric relaxer properties of ferroelectric BKT single crystal by molten salt method. They reported that the maximum in $\varepsilon_r$ is diffusive and centered at around 357 °C accompanied by a strong dispersion of dielectric maximum temperature ($T_m$) with frequency. Upon increasing the field frequency, the dielectric maximum decreases, while the Curie temperature increases (from 337 C at 1 kHz to 362 at 1000 kHz), showing the relaxer behavior of the present ceramics, as shown in Figure 16.

The polarization hysteresis behavior of BKT measured at several temperatures was also reported, as shown in Figure 17. Hysteresis loop is observed even at temperatures as high as 260 °C [64]. As expected, the coercive field also

gradually decreases with an increase in temperature, as does the remnant polarization. The remnant polarization ($P_r$ = 22.2μC/cm$^2$) and 52.5 kV/cm of BKTwere reported [66].

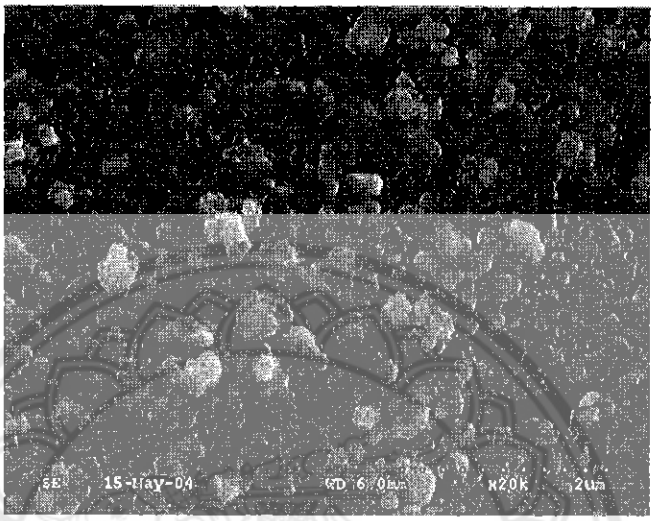


**Figure 14 FESEM micrograph of the BKT powders was studied by Hou et al. [63]**

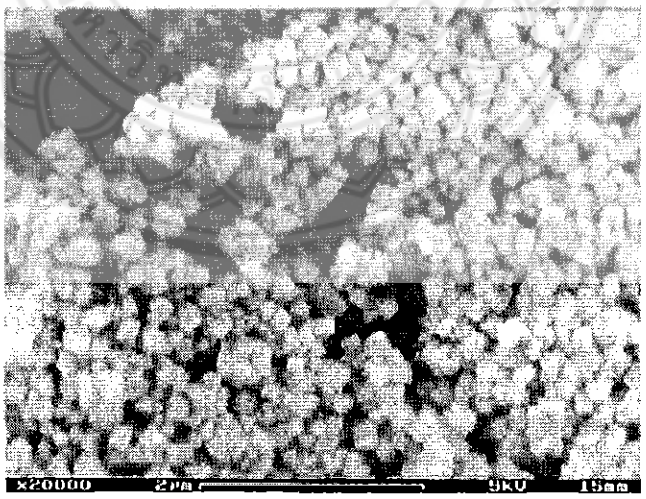


**Figure 15 FESEM micrograph of the BKT powders was studied by Lencka et al. [56]**

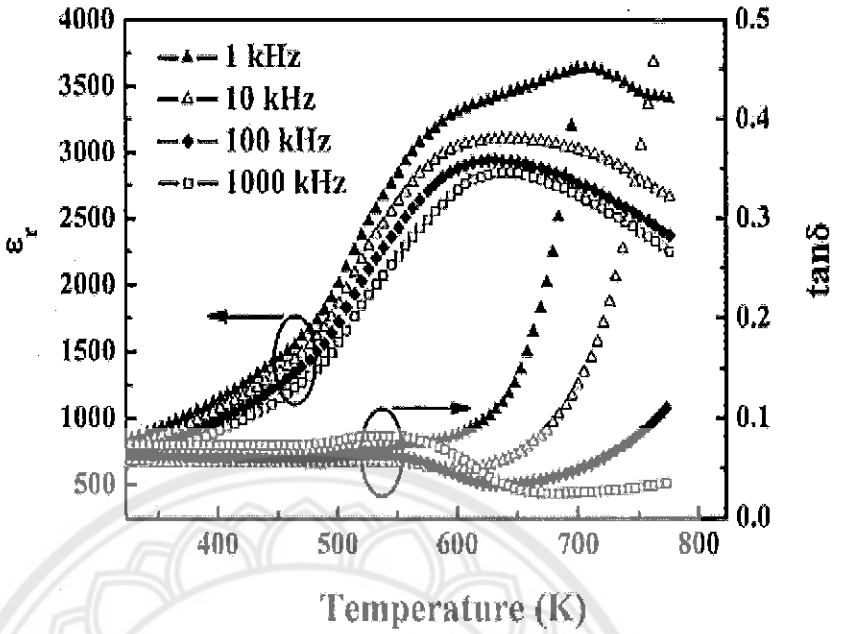


**Figure 16** Temperature dependence of dielectric constant $\varepsilon_r$ and loss tanδ at various frequencies for $(K_{0.5}Bi_{0.5})TiO_3$ ceramics [65]

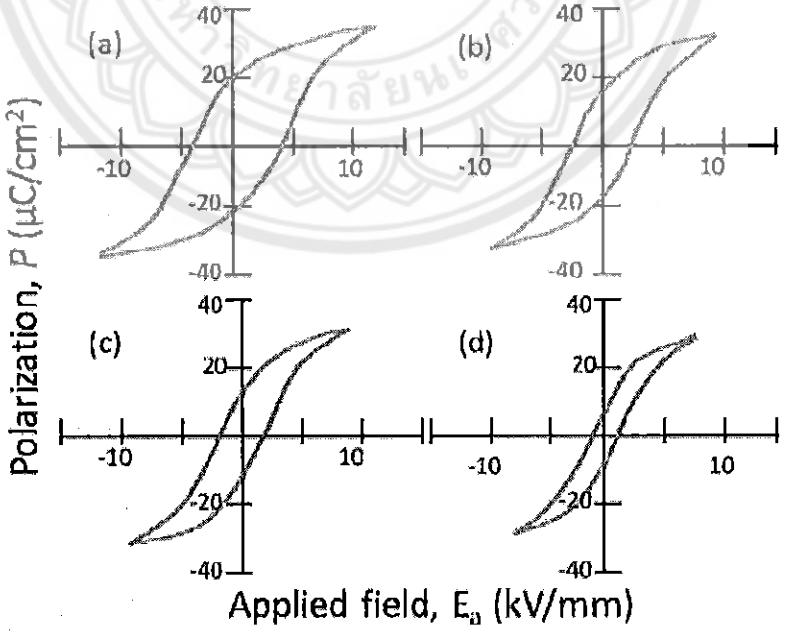


**Figure 17** Polarization of KBT measured at temperatures of (a) 100 °C, (b) 200 °C, (c) 240 °C and (d) 260 °C [66]

**Binary Systems**

For some of the lead-free systems described above, the piezoelectric properties are enhanced through the use of dopants. The enhancement of piezoelectric properties is selection of a composition near an MPB in a solid solution. This section discusses the structure and properties of several lead-free binary solid solution material compositions.

**$Bi_{0.5}Na_{0.5}TiO_3$ –$BaTiO_3$ (BNT-BT)**

$BaTiO_3$ (BT) has also been combined in a solid solution with BNT, in which case an MPB is found at 6-7 mol% BT between the ferroelectric rhombohedral and ferroelectric tetragonal phases, as shown in Figure 18. At this composition, the system exhibits improved properties relative to BNT, such as the piezoelectric constant ($d_{33}$=125 pC/N), coupling factor ($k_p$=20%), and dielectric constant ($\varepsilon_r$=580) [67].

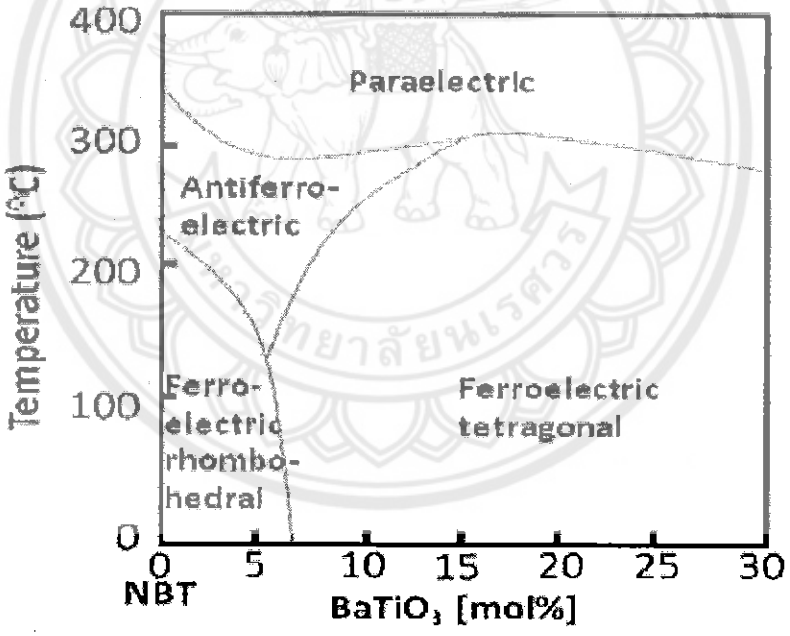


**Figure 18 Phase diagram of BNT-BT showing the MPB between the ferroelectric rhombohedral phase and the ferroelectric tetragonal phase, reproduced from Takenaka et al. [67]**

**$Bi_{0.5}Na_{0.5}TiO_3$ –$NaNbO_3$ (BNT-NN)**

BNT was also combined with $NaNbO_3$ (NN) by Li et al. [6]. They reported that the solid solution of BNT-NN forms MPB between rhombohedral ferroelectric and orthorhombic anti-ferroelectric structure in the region of 2-8 mol% NN. At the MPB, the dielectric constant at RT, dielectric loss tangentat RT, piezoelectric constant and electro mechanical coupling factor varies from 467-889, 4.11-6.26 %, 31-88 pC/N and 12.3-17.9%. Furthermore, the BNT-NN ceramics exhibited relaxer behavior which is characterized by a diffused phase transition, as shown in Figure 19.

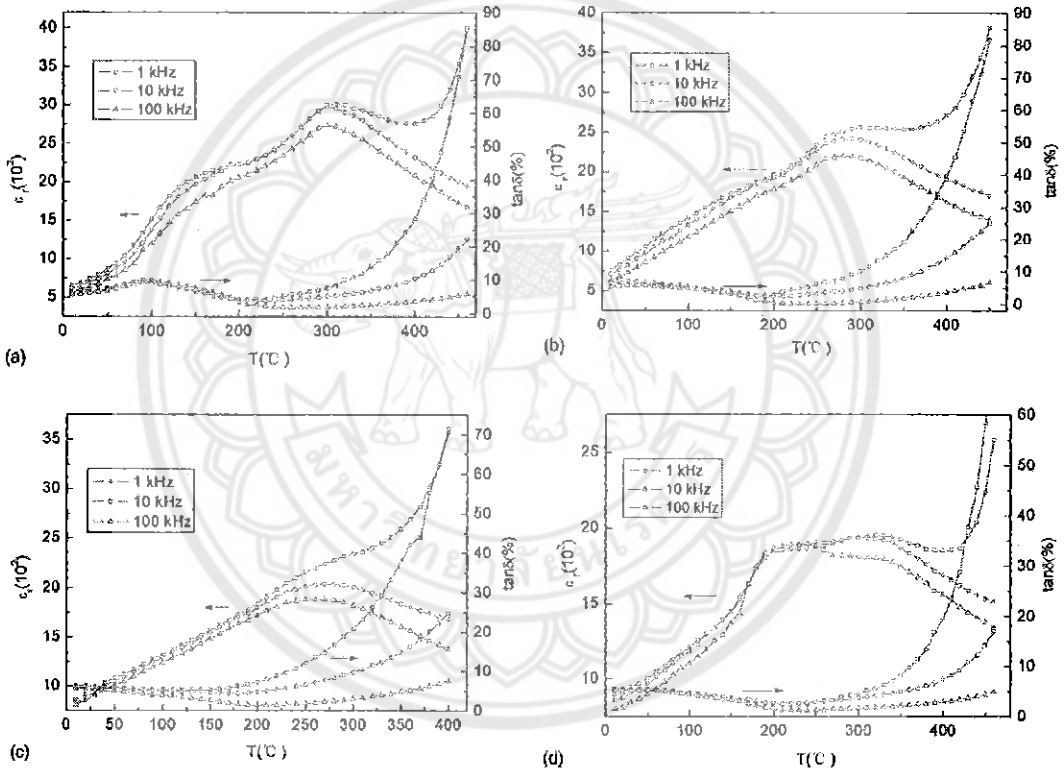


**Figure 19 Temperature dependence of dielectric constant ($\varepsilon_r$) and dielectric loss (tanδ) for (1-x)NBT–xNN ceramics at 1, 10, 100 kHz with (a) x = 0.02, (b) x =0.04, (c) x =0.06 and (d) x =0.08[6]**

**$Bi_{0.5}Na_{0.5}TiO_3$ –$Ba(Cu_{0.5}W_{0.5})O_3$ (BNT-BCW)**

For the BNT-BCW system, the structure remains a single rhombohedral phase with no MPB seen within the addition amount of BCW from 0 to 6 mol%. The addition of BCW into BNT ceramics facilitated the poling process by a reduction in leakage current. 0.995BNT-0.005BCW ceramics exhibit a relatively high piezoelectric electric constant ($d_{33}$=80 pC/N), electromechanical coupling factor ($k_p$=18.1%), dielectric constant ($\varepsilon_r$ = 328) and a relatively low dielectric loss (tanδ = 0.015) [68].

**$Bi_{0.5}Na_{0.5}TiO_3$ –$SrTiO_3$ (BNT-ST)**

BNT was also combined with ST by Watanabe et al. [7], showing an increase in the dielectric constant compared to undoped BNT, as shown in Figure20. $T_d$, $T_m$ and $T_{R-T}$ of BNT-ST ceramics was found that it shifts the lower temperature when the ST content increased as shown in Figure 21. The optimum values of $d_{33}$ is 133 pC/N obtained from 0.80BNT-0.20ST ceramics.

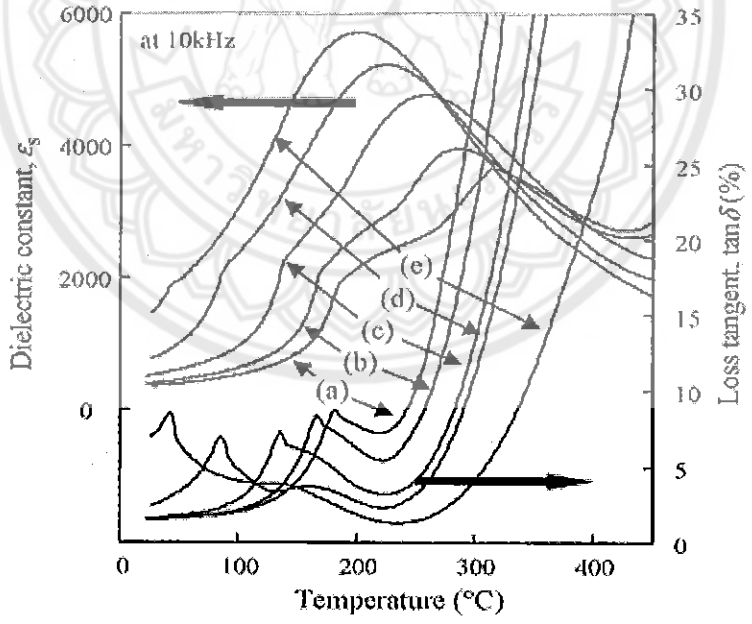


**Figure 20 The dielectric constant and tanδ of BNT-ST (a) x = 0.04, (b) x = 0.08, (c) x = 0.14, (d) x = 0.20 and (e) x = 0.24[7]**

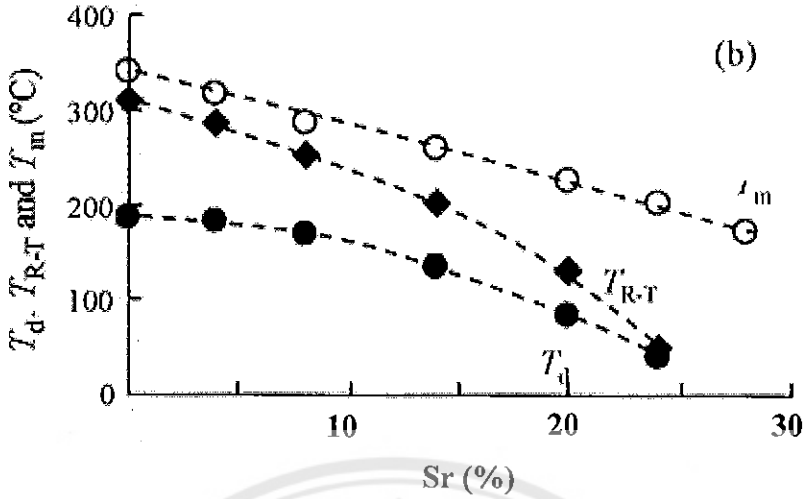


**Figure 21 $T_d$,$T_{R-T}$ and $T_m$ of BNT-ST ceramics[7]**

**$Bi_{0.5}Na_{0.5}TiO_3$-$Bi_{0.5}K_{0.5}TiO_3$ (BNT-BKT)**

The crystal structure of BNT-BKT ceramics was studied by Yang et al. [1]. They reported that a solid solution of BNT-BKT forms MPB between rhombohedral and tetragonal structure in the region of 16-22 mol % BKT. It agrees with the results of Sasaki [69].The addition of BKT into BNT ceramic caused the grain size to decrease. The density increases with increasing BKT content, the maximum density is obtained at18 mol% of BKT, as shown in Figure 22.

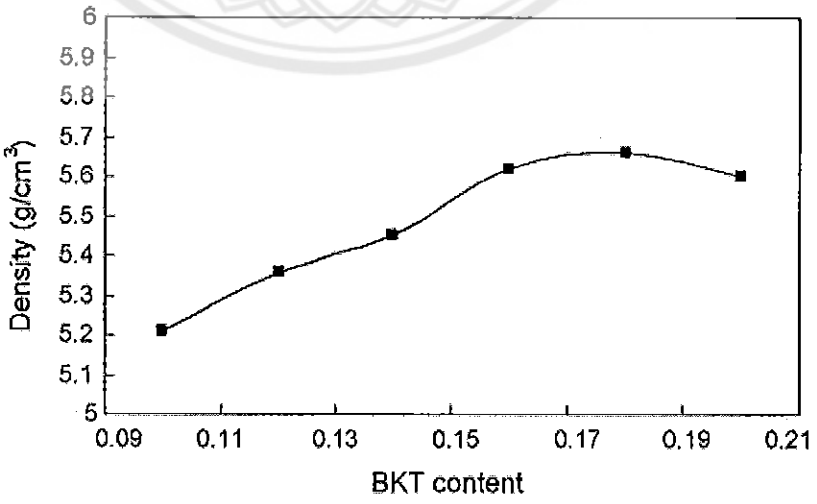


**Figure 22 Density of BNT-BKT ceramics [1]**

The dielectric constant ($\varepsilon_r$) and dielectric loss (tanδ) of BNT-BKT were also reported. The highconcentration of caused the $\varepsilon_r$ increases andthe loss tanδ to decreased. There are two abnormal temperature peaks at around 100-200 and 300-350 °C were reported. Takenka et al. [70] concluded that these dielectric anomalies are attributed to ferroelectric-antiferroelectric and antiferroelectric-paraelectric phase transitions from the shape of P-E curve. Furthermore, BNT-BKT ceramics exhibited a relaxor ferroelectric behavior, as shown in Figure 23, agrees with the results of Yasuda and Konda [71].

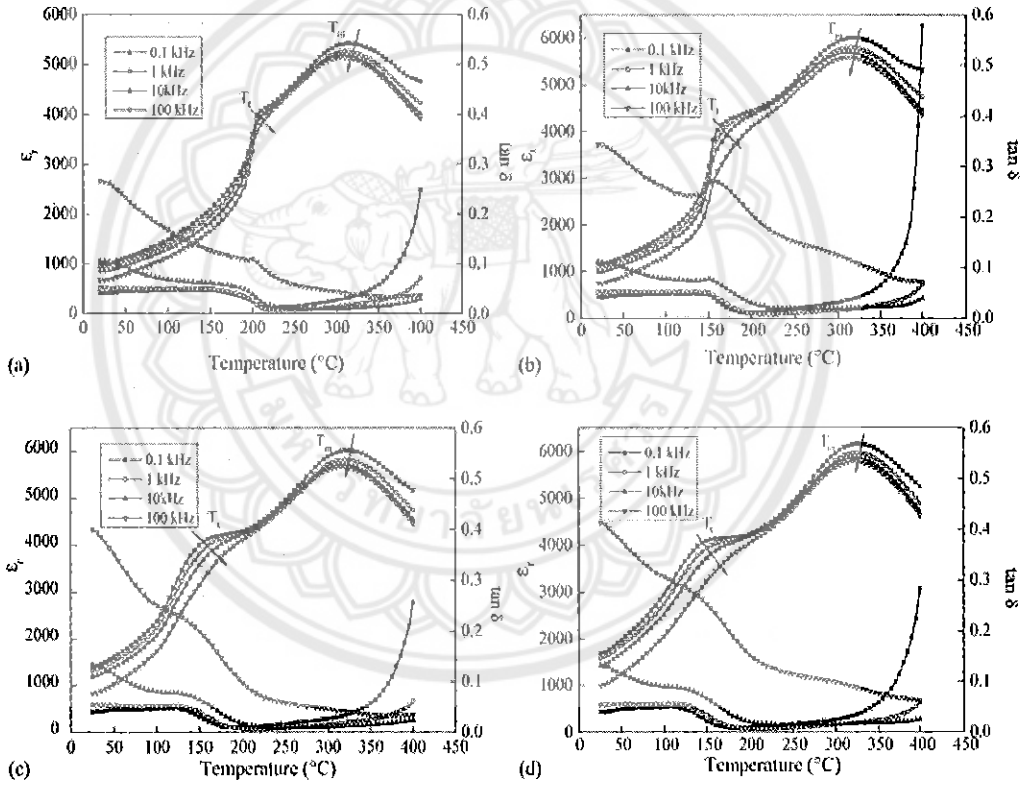


**Figure 23 The dielectric constant and dielectric loss of BNT-BKT ceramics: (a) 12 mol% of BKT (b) 16 mol% of BKT (c) 18 mol% of BKT (d) 20 mol% of BKT[70]**

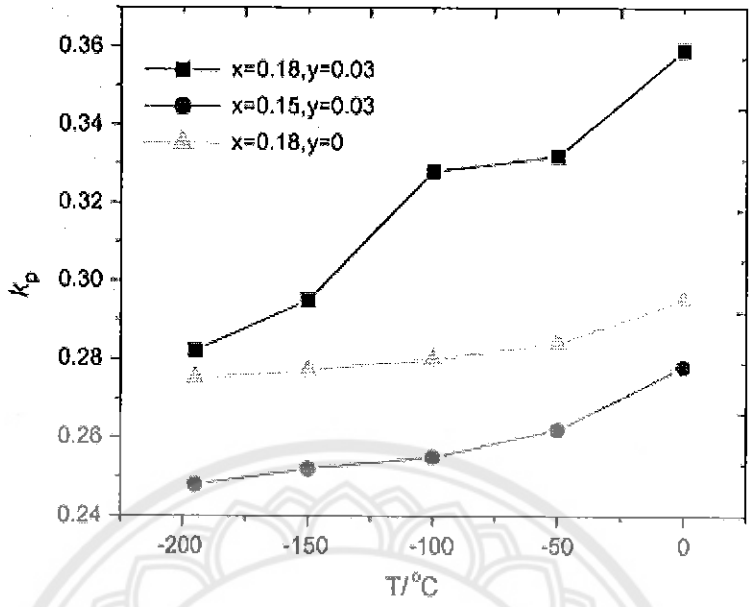


**Figure 25 The electromechanical coupling factor $k_p$ of (1−x−y)BNT–xBKT–yBF ceramics with x=0.18, y =0; x =0.18, y = 0.03 andx =0.15, y = 0.03 [19]**

**$Bi_{0.5}Na_{0.5}TiO_3$-$Bi_{0.5}K_{0.5}TiO_3$-$K_{0.5}Na_{0.5}Nb_{0.5}O_3$(BNT-BKT-KNN)**

$K_{0.5}Na_{0.5}NbO_3$(abbreviated as KNN) is a well-known lead-free piezoelectric ceramic because of its high Curie temperature ~420 °C and large electromechanical coupling factors. Recently, Yao et al. [15] added a small amount of KNN to BNT-BKT. The phase transition between rhombohedral and tetragonal phases was confirmed. The piezoelectric properties of BNT-BKT-KNN were also reported 0.75 BNT-0.22BKT0.03KNN exhibited the $d_{33}$ of 167 pC/N and $k_p$ of 35.5%, as shown in Figure 26.

Hussain et al. [81] studied the bipolar strain behavior of KNN-modified BNT-BKT measured at 0.2 Hz under an applied electric field of 50 kV/cm. They have shown BNT-BKT without KNN exhibit a butterfly-shaped curve typical of ferroelectric material with maximum and negative strains of 0.12% and 0.11%, respectively. When a small amount of KNN is introduced, the curves change shape, resulting in an increase in maximum strain and a concurrent decrease in the negative strain. At 3 mol% KNN, a significant enhancement in strain (S=0.22%). Singh et al.

The piezoelectric constant ($d_{33}$) and electromechanical coupling factor ($k_p$) of BNT-BKT were also reported. The addition of BKT into BNT ceramics increased $d_{33}$ and $k_p$. The optimum values of $d_{33}$ and $k_p$were found to be 144 pC/N, 29% at 18 mol% of BKT.

From the literature, the solid solution of BNT-BKT ceramics showed different piezoelectric properties. A comparison of the properties of BNT-BKT ceramics and BNT doping other of various groups is shown in Table 4.

**Table 4** The optimal piezoelectric constant ($d_{33}$) and electromechanical coupling factor ($k_p$) of the composition in various BNT-based piezoelectric ceramics

| BNT-based solid solution | MPB | $d_{33}$ (μC/N) | $K_p$ (%) | Ref. |
|---|---|---|---|---|
| BNT | - | 58 | 12 | [72] |
| 0.94BNT-0.06$BaTiO_3$ | o | 125 | 20 | [73] |
| 0.995BNT-0.005$Ba(Cu_{0.5}W_{0.5})O_3$ | o | 80 | 18.1 | [68] |
| 0.98BNT-0.02$NaNbO_3$ | - | 88 | 17.9 | [6] |
| 0.985BNT-0.01$EuTiO_3$ | - | 46 | - | [74] |
| $(Bi_{0.5}Na_{0.5})_{0.9742}La_{0.0172}TiO_3$ | - | 91 | 13 | [75] |
| 0.98BNT-0.02$BiScO_3$ | - | 74 | 14.4 | [76] |
| 0.99BNT-0.01$CaTiO_3$ | - | 50 | 13.8 | [7] |
| 0.993BNT-0.007$Bi(Mg_{2/3}Nb_{1/3})O_3$ | - | 94 | - | [77] |
| 0.994BNT-0.006$BaNb_2O_6$ | - | 94 | - | [78] |
| 0.88BNT-0.12$PbTiO_3$ | o | 106.6 | 33.2 | [79] |
| 0.82BNT-0.18$Bi_{0.5}K_{0.5}TiO_3$ | o | 144 | 29 | [1] |

**Ternary Systems**

As the binary systems described above still have many drawbacks and are not capable of replacing PZT in all of its applications, new lead-free compositions have become even more complex through the use of ternary solid solutions.

**$Bi_{0.5}Na_{0.5}TiO_3$-$Bi_{0.5}K_{0.5}TiO_3$-$BiFeO_3$(BNT-BKT-BF)**

Several reports have been made by Zhou et al. for the BNT-BKT-BF ternary system. The MPB in this system is between rhombohedral and tetragonal phases, where composition of $0.18<x<0.21$ and $0<y<0.05$ in (0.97-x)BNT-xBKT-0.03BF and (0.82-y)BNT-0.18BKT-yBF [18] respectively. Zou et al. [80] studied the microstructure of BNT-BKT-BF ceramics by SEM technique. They reported that the addition of BF into BNT-BKT caused bulk sample increased and promotegrain growth.

Measurement of the dielectric constant $\varepsilon_r$, piezoelectric constant $d_{33}$ and the planar electromechanical coupling factor $k_p$ of BNT-BKT-BF ceramics were studied by Zhou et al. [19]. The $\varepsilon_r$,$d_{33}$ and $K_p$ increased with increasing BF into BNT-BKT ceramics. The ceramics were found to exhibit a typical relaxor behavior. 0.79BNT-0.18BKT-0.03BF ceramics demonstrated the largest $d_{33}$ and $k_p$ are 170 $pCN^{-1}$ and 36.6 %, as shown in Figure 24 (a) and (b) and Figure25, which shows that ceramics are very promising lead-free piezoelectric materials.

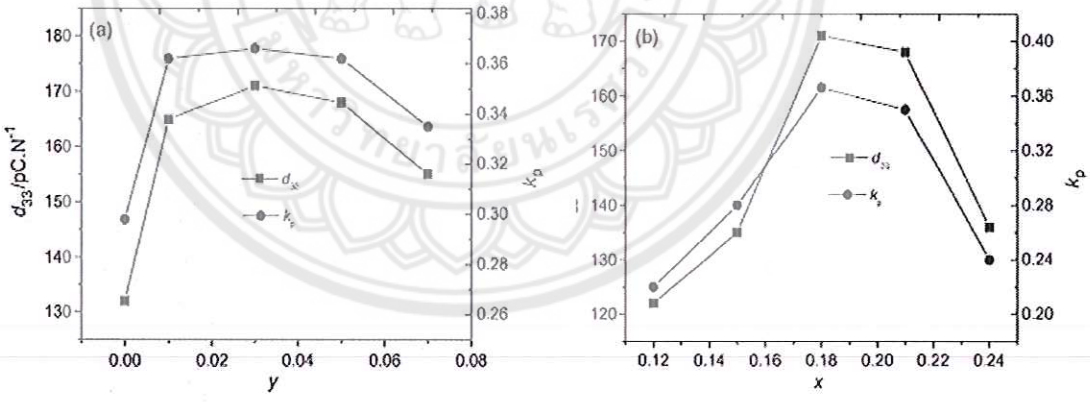


(a) (b)

**Figure 24 Piezoelectric constant $d_{33}$ and planar lectromechanical coupling factor $k_p$ of (1−x−y)BNT–xBKT–yBF ceramics as a function of the amount of BKT and BF: (a) x = 0.18 and (b) y = 0.03 [19]**

[82] studies the BNT-BKT-KNN ternary system by conventional solid state method. 0.80BNT-0.20BKT-0.01KNN exhibited the largest strain ever reported for a polycrystalline lead-free ceramics, ~0.80%, as shown in Figure 27, which is even higher than the strain obtained with established ferroelectric $Pb(Zr,Ti)O_3$ ceramics and is comparable to strains obtained in Pb-based antiferroelectrics.

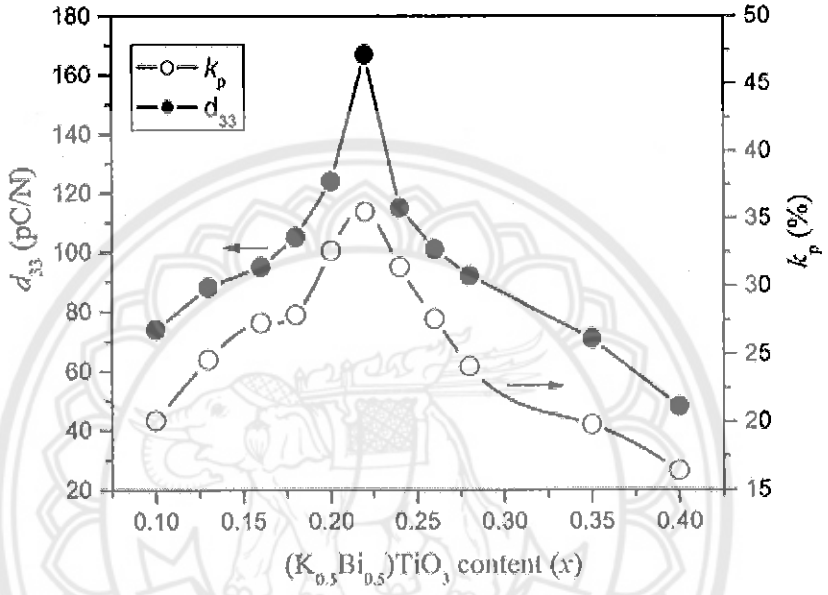


**Figure 26 Piezoelectric coefficient $d_{33}$ and planar coupling factor $k_p$ of (1-x-y)BNT-xBKT-0.30KNN at x = 0.10–0.40 [15]**

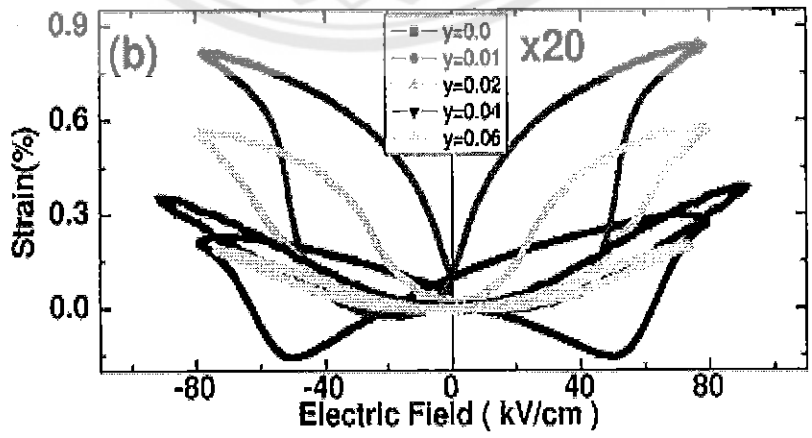


**Figure 27 Bipolar strain vs electric field of 0.80BNT-0.20BKT-0.01KNN ceramic at room temperature at 1 Hz [82]**

**$Bi_{0.5}Na_{0.5}TiO_3$-$Bi_{0.5}K_{0.5}TiO_3$-$Bi_{0.5}Li_{0.5}TiO_3$(BNT-BKT-BLT)**

Lin et al. [83] also studied the solid solution of BNT-BKT-BLT near the MPB. The ceramics were prepared by solid state reaction method and investigated by X-ray diffraction and for piezoelectric properties. The XRD patterns showed the MPB of therhombohedral phase and tetragonal phase. 0.70BNT-0.20BKT-0.10BLT demonstrated that the excellent piezoelectric constant and planar coupling factor of 231 pC/N and 41%, as shown in Figure 28. Hiruma et al. [84] added a small amount of KNN to BNT-BKT. The addition of BLT decreases greatly the sintering temperature and assists in the densification of BNT-BKT ceramics. The depolarization temperature ($T_d$) shows a strong dependence on the concentration of BLT and reaches the highest values at the MPB. These results show that the BNT-BKT-BLT ceramics are promising candidates for the lead-free materials.

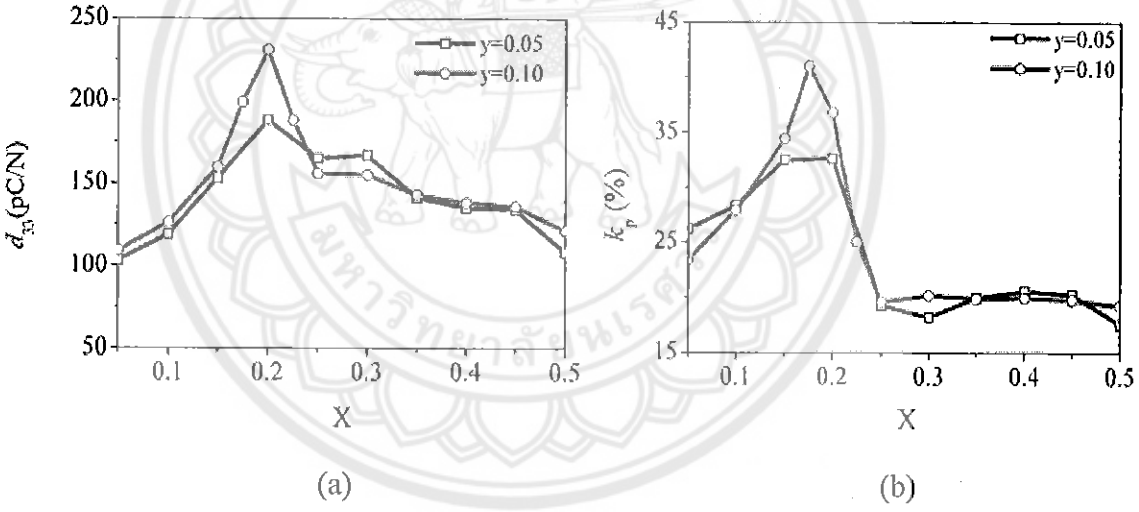


**Figure 28 Variation of piezoelectric coefficient $d_{33}$ and planar electromechanical coupling factor $k_p$ with x for the (1-x-y)BNT-xBKT-yBLT ceramics (y=0.05 and 0.10) [83]**

# CHAPTER III

## MATERIALS AND METHOD

In this chapter, the experimental procedures employed for preparation and characterization of BNT-BKT-based ceramics are described. The ternary system piezoelectric ceramics of $0.77Bi_{0.5}Na_{0.5}TiO_3$–$0.02Bi_{0.5}K_{0.5}TiO_3$–$0.03(Na_{0.5}K_{0.5})NbO_3$ , (abbreviated as BNKNT-0.20/0.03) are prepared in this work. The details are presented in the following sections.

**Sample Preparation**

Fabrications of materials, including powder preparation and ceramics fabrication have been described as follow:

**Preparation of BNNKT-0.20/0.03 powders**

The ternary system BNNKT-0.20/0.03 was synthesized by combustion method. Reagent grade $Bi_2O_3$, $NaCO_3$, $Nb_2O_5$, $K_2CO_3$ and $TiO_2$ were used as starting materials. The details of these oxides; such as the supplier, formula weights and purities, are listed in Table 5. First, these oxides or carbonate powders were weighed in appropriate stoichiometry. The ball-milling technique was employed for the mixing and milling in this work. The powders were mixed by ball milling for 24 h. with ethanol as a solution media. Drying was carried out on a hotplate with a magnetic stirring until the mixture nearly dry, and then placed in a 120 °C drying oven for 2 h. The suspensions were dried and the powders were ground using an agate mortar and then sieved into a fine powder. The mixed powders and glycine ($C_2H_5NO_2$) were mixed with a ratio of 1:2 in an agate mortar. The BNKFT, BNKNT and BNKLT powders were then calcined at various temperatures until the optimum condition was determined.The calcined powders were analyzed by X-ray diffraction technique to determine the amount of the perovskite phase percentage.

**Table 5 Specifications of starting materials used in this study**

| Materials | Source | Formula weight | Purity (%) |
|---|---|---|---|
| $Bi_2O_3$ | Qrec | 208.98 | 99.5% |
| $NaCO_3$ | Riedel-de Haën | 22.99 | 99.5% |
| $TiO_2$ | Sigma-Aldrich | 47.90 | 99.5% |
| $K_2CO_3$ | Riedel-de Haën | 39.10 | 98.0% |
| $Nb_2O_5$ | Eleps | 92.91 | >99.95% |

**Preparation of BNNKT-0.20/0.03 ceramics**

The calcined powders received from the processes described in previous sections were mixed with 3 wt.% polyvinyl alcohol (PVA, Fluka) which was used as binder. The mixed powders were pressed by uniaxial hydraulic press to form disc-shaped pellets 10 mm in diameter. Binder was burned out on sintering step at temperature 500 °C for 1 h. The green pellets were placed on the alumina powders-bed inside alumina crucible, before insertion into a high temperature furnace.

**Sample Characterization**

All powders and ceramics were characterized using different tools as described below in Figure 29.

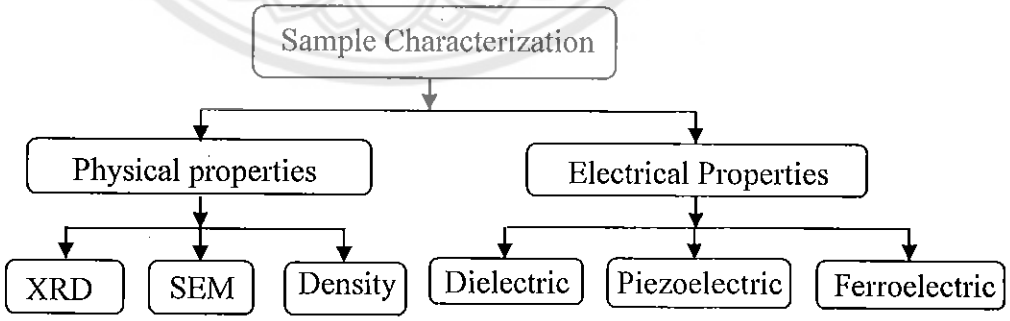


**Figure 29 Diagram of experimental procedure on sample characterization**

The X-ray diffraction (XRD) was used to analyze phase formation and phase purity which was especially important in minimizing pyrochlore phase formation in BNT-BKT-based powders and pellets. The room temperature XRD patterns were

recorded with a Siemens-D500 diffractometer at Naresuan University with Cu Kαradiation at 20 kV. The relative amounts of the perovskite and pyrochlore phases were estimated from these major peak intensities (110) or the respectively phases. The estimation was suggested by Swartz and Shrout [85] using the following equation:

$$\%\ perovskite\ phase = \left( \frac{I_{perov}}{I_{perov} + I_{Pyr}} \right) \times 100 \qquad (6)$$

This well-known equation is widely employed in connection with the preparation of complex perovskite structure materials. $I_{perov}$ referred to the intensity of the (110) perovskite peak, intensities of the highest, $I_{pyr}$ peaks.

**Scanning Electron Microscopy (SEM)**

Microstructural characterization of sample surface using scanning electron microscopy (SEM) was performed to determine the grain size and the presence of porosity. Average grain size of the sintered ceramics were estimated by using a linear intercepting method [86,87], where random lines were drawn on a micrograph and the number of grain boundaries intercepting these lines were then counted.

**Densification Measurement**

The method of measuring the density of a piece of ceramics material usually described in standards is based on the Archimedes principle [87]. This principle stated the weight of an object in a fluid equals it's by weight minus the buoyant force (or the weight of the fluid displaced). However, it is usual to measure open porosity levels at the same time by ensuring that during immersion liquid can penetrate all parts of the specimen through the open porosity. Typical procedures are;

1. Dry specimen(s) in air at 110 C, store in a desiccator, weigh when cold (mass $W_1$)

2. Boil in distilled water for a period, typically 3 hoursand leave it for 1 night

3. Weigh immersed in water ($W_2$) and then weight during immersion liquid can penetrate all parts of the specimen through the open porosity ($W_3$).

4. Calculate follow this equation:

$$\rho_c = \frac{W_1 \rho_w}{W_3 - W_2} \quad (7)$$

where, $\rho_w$ is the density of water at room temperature ($g/cm^3$) and is the density of sample at room temperature ($g/cm^3$); however the density of water is slightly temperature dependent

$$\rho_w = 1.0017\text{-}0.0002315T \quad (8)$$

**Electrical properties**

**I. Dielectric Measurement**

The dielectric properties of the sintered ceramics were studied as functions of both temperature and frequency with an automated dielectric measurement system. The computer-controlled dielectric measurement system consists of a precision LCR-meter (Agilent 4263B), a temperature chamber, and a computer system. The capacitance and the dielectric loss tangent are determined over the temperature range of 50 and 500 °C with difference frequency.

The dielectric constant was calculated by equation,

$$\varepsilon_r = \frac{Ct}{\varepsilon_0 A} \quad (9)$$

Where $\varepsilon_r$ and $\varepsilon_0$ are the dielectric constant and permittivity of free space. C is thecapacitance, and t and Aare the thickness and area of the sample.

**II. P-E and S-Eproperties measurement**

P-E and S-Emeasurements were made using high voltage amplifier (Trek), precision High Voltage Interface (HVI, Radiant Technologies), precision LC (Radiant Technologies) and computerized control and data acquisition. The sample is placed in a High Voltage Test Fixture chamber (HVTF) chamber in bottom half of the fixture. A copper electrode fixed in the bottom of the chamber contacts the electrode on

the bottom of the sample. The bottom chamber is sealed so it may be filled with insulating oil to protect the sample from the arcing that may occur in open air. The system is an automated device intended for measuring the polarization of materials induced by a single triangle wave. It can prevent the excess voltage and current during a sample breakdown from exceeding the current canceling capability of the virtual ground circuitry on the tester input. During the measurement, an electric field of 10-60 kV/cm based on the coercive field was applied to a sample which immersed in a silicone oil to prevent the breakdown of the sample

The high field $d_{33}^*$ was calculated as the ratio of the maximum strain to the maximum field in the cycle, according to this equation,

$$d_{33}^* = \frac{S_{max}}{E_{max}} \tag{10}$$

where $S_{max}$ and $E_{max}$ are maximum strain and maximum field in the cycle

**III. Piezoelectric properties measurement**

The optimum poling conditions were determined by poling the ceramics with applying DC field of 5 kV/mm in a stirred oil bath at 120 °C for a time period 30 minutes. The piezoelectric constant ($d_{33}$) was measured using a quasi-static piezoelectric $d_{33}$ meter. The piezoelectric constant ($d_{33}$) measurements were made directly after poling and after 24 hours. Measurements were conducted at a drive frequency of 100 Hz.

# CHAPTER IV

# RESULTS AND DISCUSION:

## $0.77Bi_{0.5}Na_{0.5}TiO_3–0.02Bi_{0.5}K_{0.5}TiO_3–0.03(Na_{0.5}K_{0.5})NbO_{33}$

### The influence of firing temperatures on crystal structure and microstructure of BNNKT ceramics

The XRD patterns of BNNKT-0.20/0.03 powders with various calcination temperatures between 600 °C and 850 °C for 2 h are shown in Figure 30. The crystal structure belonged to rhombohedral matched with JCPDS file number 360340. At temperature < 750 °C, an impurity phase of $K_4Ti_3O_8$ was discovered (Figure 30(a)).The pure perovskite phase was found at the calcination temperature ≥ 750 °C, as shown in Figure 30.The percent perovskite phase of BNNKT can be calculated by the following equation (11). When $I_{perov}$ and $I_{K_4Ti_3O_8}$ are the intensity of the (110) perovskite and the intensity of the highest $K_4Ti_3O_8$ peak. The percent of the perovskitephase of BNNKT-0.20/0.03 powders at various calcination temperatures wascalculated and is listed in Table 7.The percent perovskite phase in all samples increased with an increase of the calcination temperaturesand the highest percentage was observed in powders calcinedabove 750 °C.

$$\%\,Perovskite\ phase = \left(\frac{I_{Perov}}{I_{Perov} + I_{K_4Ti_3O_8}}\right) \times 100 \qquad (11)$$

Figure 31 shows the XRD diffraction pattern of BNNKT sintered ceramics at various temperatures. The pure perovskite phase was found in all ceramic samples. All the peaks of the solid solution system were indexed by pattern matching based on JCPDS data on BNT (36-0340) and $Bi_{0.5}K_{0.5}TiO_3$ (36-0339). At sintering temperature of 900 °C, splitting of a (003)/(021) peaks was detected in the 2θ range of 39-41° (Figure 31(b)) and the (202) peak is asymmetric in the range of 45-48° (Figure 31(c)). When sintering temperature is increased, the (003)/(021) peak begins to merge into

a single (111) peak and the (202) peak starts to split into two peaks of (002)/(200). This characterizes indicated the coexistence of rhombohedral and tetragonal phases, which is consistent with the nature of the specimen with an MPB composition.

The SEM photographs of BNNKT-0.20/0.03 calcined powders at various temperatures are shown in Figure 32. It was found that the particle size exhibited spherical morphology. With increase in sintering temperature, the particle size trend to increase. The average particle size increased from 226 nm to 326 nm for BNNKT 0.20/0.03 with an increase of calcination temperature from 600°C to 850°C and is listed in Table 7.

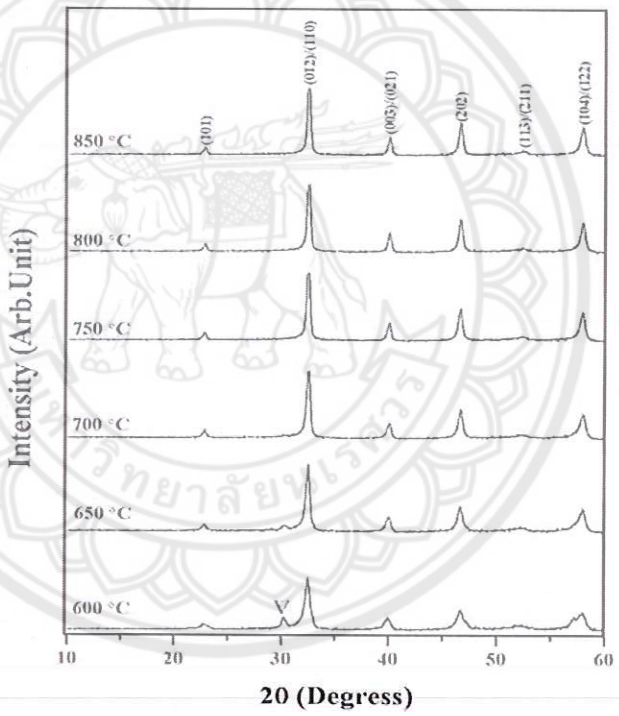


**Figure 30 XRD patterns of BNNKT0.20/0.03 powders calcined at various temperatures for 2 h: (∇ $K_4Ti_3O_8$)**

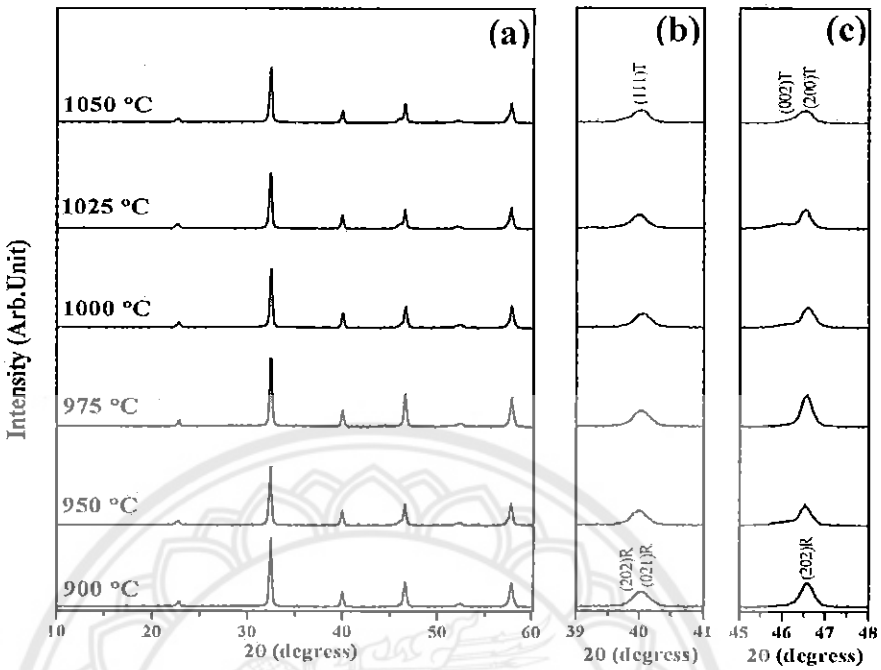


**Figure 31** X-ray diffraction patterns of BNNKT-0.20/0.03 sintered ceramics in the 2θ range of (a) 10° to 60°, (b) 39° to 41° and (c) 45° to 48°

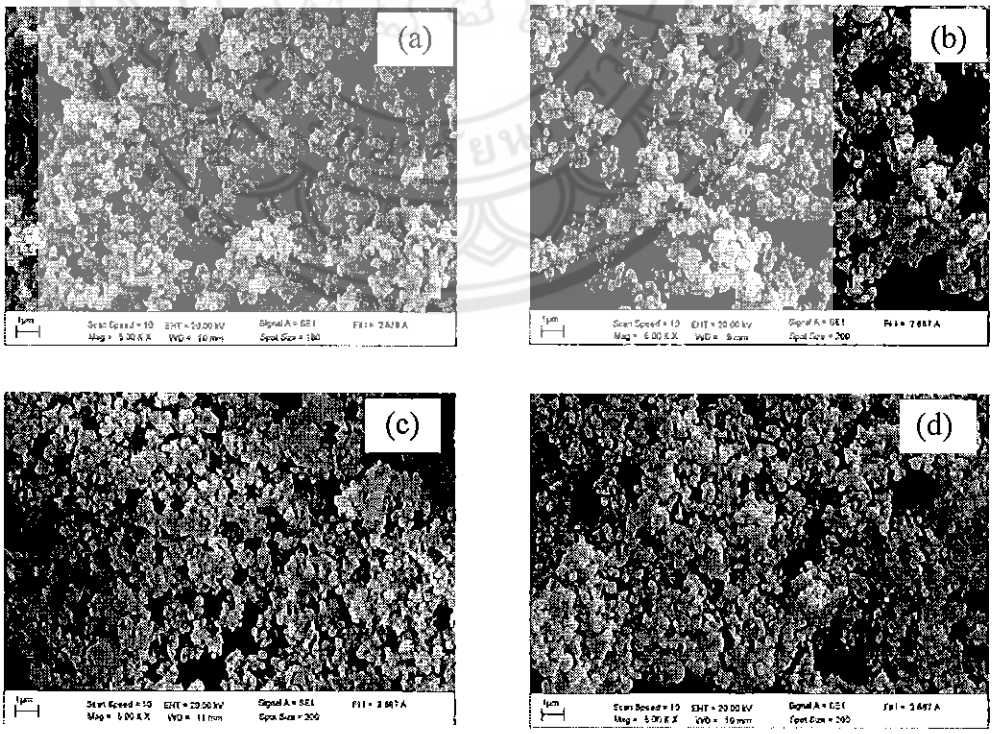


**Figure 32** SEM images of BNNKT-0.20/0.03 calcined at (a) 600 °C, (b) 700 °C, (c) 800 °C and (d) 850 °C

**Table 7 Percent perovskite phase, lattice parameter a, average particle size, average grain size, density and shrinkage of BNNKT**

| Calcination Temperature (°C) | Calcined powder | | | Sintering Temperature (°C) | Sintered ceramic | | | |
|---|---|---|---|---|---|---|---|---|
| | Perovskite phase (%) | Lattice parameter (Å) | Average particle size (nm) | | Average grain Size (μm) | Measured density ($g/cm^{-3}$) | Relative density (%) | Shrinkage (%) |
| 600 | 79.5 | 3.8012±0.034 | 226±15.3 | 900 | 0.66 | 4.74 | 79.8 | 10.0 |
| 650 | 92.1 | 3.8166±0.066 | 249±10.4 | 950 | 0.70 | 5.21 | 87.8 | 11.3 |
| 700 | 95.2 | 3.8247±0.036 | 277±12.4 | 1000 | 0.82 | 5.37 | 90.5 | 13.9 |
| 750 | 100 | 3.8578±0.093 | 312±17.4 | 1025 | 1.13 | 5.64 | 95.5 | 16.4 |
| 800 | 100 | 3.8604±0.031 | 326±14.2 | 1050 | 1.29 | 5.41 | 91.2 | 15.0 |

# CHAPTER V

# SUMMARY

BNKLT ceramics were prepared by the combustion technique with optimum calcination and sintering of 750 and 1025 for 2 h. The firing temperatures have direct effect on phase formation, grain size, densification microstructure and dielectric properties of ceramic samples. The structure exhibited the coexistence of rhombohedral and tetragonal phases, which is consistent with the nature of the specimen with an MPB composition. The optimum sintering temperature significantly promoted the grain growth and microstructure densification. The highest dielectric at $T_c$ ($\varepsilon_r$ = 4,344) and density ($\rho$ = 5.79 g/cm$^{-3}$) were obtained from the sample sintered at 1025 °C. These results were higher than the sample obtained by solid state reaction method and confirmed that the combustion technique has potential to fabrication of high purity BNKLT ceramics using lower firing temperature.

[21] Julphunthong P. and Bongkarn, T. (2013). Phase formation, microstructure and dielectric properties of $Ba(Zr_{0.1}Ti_{0.9})O_3$ ceramics prepared via the combustion technique. **Current Applied Physics**, 39, S415.

[22] Chaimongkon, U., Thongtha, A. and Bongkarn, T. (2011). The effects of firing temperatures and barium content on phase formation, microstructure and dielectric properties of lead barium titanate ceramics prepared via the combustion technique. **Current Applied Physics**, 11, S70.

[23] Thongtha, A. and Bongkarn, T. (2009). Phase Formation and Microstructure of Barium Zirconate Ceramics PreparedUsing the Combustion Technique. **Ferroelectrics**, 383, 33.

[24] Pampuch, R. (1999). Advanced HT Ceramic Materials via Solid Combustion. **Journal of European Ceramics Societies**, 19, 2395.

[25] A.G. Merzhanov. (1996). Combustion processes that synthesize materials. **Journal of Materials Processing Technology**, 56, 222.

[26] Patil, K.C., Aruna S.T. and Mimani, T. (2002). Combustion synthesis: an update **Current Opinion Solid State Mater Sciences**, 6, 507.

[27] Wul, B.M. and Goldman, I.M. (1945). Dielectric constants of titanate of matals of the second grop. **Doklady Akademii Nauk SSSR**, 46, 154.

[28] Hippel, A.V., Breckenridge, R.G. Chesley, F.G. and Tisza, L. (1946). High dielectric constant ceramics. **IndustrialEngineering Chemical Research**, 38, 1097.

[29] Haertling, H. (1999). Ferroelectric Ceramics: History and Technology. **Journal American Ceramic Societies**, 82, 797.

[30] Jaffe, B. Cook, W.R. and Jaffe, H. (1971). **Piezoelectric ceramics**. India: Ceramic Book and Literature Service.

[31] Moulson A.J. and Herbert, J.M. (2003). **Electroceramics**. New York: Wiley- Interscience.

[32] Yuhuan, X. (1991). **Ferroelectric materials and their applications.** Natherland: Elsevier Science Publishers B.V.

[32] Fousek, J. (1995). Joseph Valasek and the Discovery of Ferroelectricity. **Proceeding of the IEEE**, 1.

[33] Sawyer, C. B. and Tower, C. H. (1930). Rochelle Salt as a Dielectric. **Physics Review**, 35, 269.

[34] Chiang, Y. Birnie, M.D.P. and Kingery, W. D. (1997). **Physical ceramics.** New York: John Wiley & Sons.

[35] Jaffe, B. Cook W. R. and Haffe, H. (1971). **Piezoelectric ceramics.** New York: Academi Press.

[36] Jona F. and Shirane, G. (1962). **Ferroelectric crystal.** New York: Pergamum Press.

[37] Megaw, H. (1957). **Ferroelectricity in crystals.** London: Methuen.

[38] Uchino, K. (1997). **Piezoelectric actuators and ultrasonics motors.** Boston: Kluwer Academic Publishers.

[39] Smolenskii, G. A. Isupov, V. A. and Agranovskaya, A. I. (1958). New Ferroelectrics of Complex Composition of the Type $A^{2+}(BI^{3+}BII^{5+})O_6$ I. **Soviet Physics Solid State**, 1, 150.

[40] Jo, W., Dittmer, R., Acosta, M., Zang, J., Groh, C., Sapper, E., Wang, K., and Rodel, J. (2012). Giant electric-field-induced strain in lead-free ceramics for actuator applications-status and perspective. **J. Electroceramics**, 29, 27.

[41] Randall, C. A. and Bhalla, A. S. (1990). Nanostructure-Property Relations in Complex Lead Perovskites. **Japanese Journal of Applied Physics**, 29, 327.

[42] Kittel, C. (1951). Theory of Antiferroelectric Crystals. **Physics Review**, 82, 729.

[43] Chiang, Y. (1997). **Physical ceramics.** New York: John Wiley & Sons.

[44] Guo, R. (2000). Origin of the high piezoelectric response in $PbZr_{1/x}$ $TiO_3$. **Physics Review Letters**, 84, 5423.

[45] Jaffe, E., Cook, W.R. and Jaffe, H. (1971). **Piezoelectric ceramics**. New York: Acadamic Press.

[46] Rahaman, M.N. (1995). **Ceramics processing and sintering**. New York: Dekker Inc.

[47] Ganguli, D. and Chatterjee, M. (1997). **Ceramic powder preparation**. USA: Kluwer Academic Publishers.

[48] Cahu, R.W., Haasen, P. and Kramer, E.J. (1996). **Materials sciences and technology**. Germany: The Federal Republic of Germany.

[49] Pierre, A.C. (1998). **Introduction to so-gel processing**. USA: Kluwer Acadamic Publishers.

[50] Ring, T.A. (1996). **Fundamentals of ceramics powder processing and synthesis**. New York: Acdemic Press Inc.

[51] Hwang, C.C., Wu, T.Y., Wan, J. and Tsai J.S. (2004). Development of novel combustion synthesis method for synthesizing of ceramic oxide powders. **Materials Science and Engineering B**, 111, 49.

[52] Wang, X.X., Tang, X.G., Kwok, K.W., Chan H.L.W. and Choy, C.L. (2005). Effect of excess $Bi_2O_3$ in the electrical properties and microstructure of $(Bi_{0.5}Na_{0.5})TiO_3$ ceramics. **Applied Physics A,** 80, 1071.

[53] Hiruma, Y., Nagata, H. and Takenaka, T. (2009). Thermal depoling process and piezoelectric properties of bismuth sodium titanate ceramics. **Journal of Applied Physics**,105, 084112.

[54] Lee, W.C., Huang, C.Y., Tsao, L.K. and Wu, Y.C. (2009). Chemical composition and tolerance factor at the morphotropic phase boundary in $(Bi_{0.5}Na_{0.5})TiO_3$-based piezoelectric ceramics. **Journal of Europeans Ceramics Societies**, 29, 1443.

[55] Lencka, M.M., Oledzka, M. and Riman, R.E. (2000). Hydrothermal synthesis of sodium and potassium bismuth titanate. **Chemistry Materials**, 12, 1323.

[56] Saradhi, B.V.B., Srinivas, K., G. Prasad and Suryanarayana, S.V. (2003). Impedance spectroscopic studies in ferroelectric $(Bi_{0.5}Na_{0.5})TiO_3$. **Materials Sciences EngineeringB**, 98, 10.

[57] Zuo, R. Su, S., Wu, Y. Fu, J., Wang, M. and Li, L. (2008). Influence of A-site nonstoichiometry on sintering, microstructure and electrical properties of $(Bi_{0.5}Na_{0.5})TiO_3$ceramics. **Material Chemistry Physics**, 110, 311.

[58] Xu, C., Lin, D. and Kwok, K. W. (2008). Structure, electrical properties and depolarization temperature of $(Bi_{0.5}Na_{0.5})TiO_3$-$BaTiO_3$lead-free piezoelectric ceramics. **Solid State Sciences**, 10, 934.

[59] Smolenskii, G.A., Isupov, V.A., Agranovskaya, A.I., Krainik, N.N. (1961). New Ferroelectrics of Complex Composition. **Soviet Physics-Solid State**, 2, 265.

[60] RaO, P.V.B. and Sankaram, T.B. (2010). Impedance spectroscopy studies of $K_{0.5}Bi_{0.5}TiO_3$. **Journal of Electroceramic**, 25, 60.

[61] Ivanova, V.V., Kapyshev, A.G., Venevtsev, Y.N. and Zhdanov, G.S. (1962). X-ray determination of the symmetry of elementary cells of the ferroelectric materials $(K_{0.5}Bi_{0.5})TiO_3$ and $(Na_{0.5}-Bi_{0.5})TiO_3$ and of high-temperature phase transitions in $(K_{0.5}Bi_{0.5})TiO_3$**. Izvestiya Rossiiskoi Akademii Nauk SSSR**, 26, 798.

[62] Hou, Y., Zhu, M., Hou, L., Liu, J., Tang, J., Wang H. and Yan, H. (2005). Synthesis and characterization of lead-free $K_{0.5}Bi_{0.5}TiO_3$ferroelectrics by sol-gel technique. **Journal Crystal Growth**, 273, 500.

[63] Hiruma, Y., Aoyagi, R., Nagata H. and Takenaka, T. (2005). Ferroelectric and piezoelectrics of $(K_{0.5}Bi_{0.5})TiO_3$ceramics. **Journal of Applied Physics**, 44, 5040.

[64] Yang, J., Hou, Y., Wang, C., Zhu, M. and Yan, H. (2007). Relaxor behavior of $(K_{0.5}Bi_{0.5})TiO_3$ceramicsderived from molten salt synthesized single-crystalline nanowires. **Applied Physics Letter**, 91, 023118.

[65] Hiruma, Y., Marumo, K., Aoyagi, R., Nagata H. and Takenaka, T. (2008). Ferroelectric and piezoelectric properties of $(K_{0.5}Bi_{0.5})TiO_3$ceramics fabricated by hot-pressing method. **Journalof Electriceramic**, 21, 296.

[66] Takenaka, T., Maruyama, K. and Sakata, K. (1991). $(Bi_{0.5}Na_{0.5})TiO_3$-$BaTiO_3$ System for Lead-Free Piezoelectric Ceramics. **Japanese Journal of Applied Physics**, 130, 2236.

[67] Wang, X. Chan, H.L.W. and Choy, C.L. (2003). $(Bi_{0.5}Na_{0.5})TiO_3$-$Ba(Cu_{0.5}W_{0.5})O_3$ Lead-free piezoelectric**. Journal of American Ceramics Societies**, 86, 1809.

[68] Sasaki, A., Chiba, T., Mamiya, Y. and Otsuki, E. (1999). Dielectric and Piezoelectric Properties of $(Bi_{0.5}Na_{0.5})TiO_3$–$(Bi_{0.5}K_{0.5})TiO_3$ Systems. **Japanese Journal of Applied Physics**, 38, 5564.

[69] Takenaka, T., Nagata, H. and Hiruma, Y. (2009). Phase Transition Temperatures and Piezoelectric Properties of $(Bi_{0.5}Na_{0.5})TiO_3$-and $(Bi_{0.5}K_{0.5})TiO_3$-Based Bismuth Perovskite Lead-Free Ferroelectric Ceramics. **IEEE Transducer Ultrasonic Ferroelectrics FrequencyControl**, 56, 1595.

[70] Yasuda N. and Konda, J. (1995). Successive paraelectric-antiferroelectric-ferroelectric phase transitions in highly ordered perovskite lead ytterbium tantalite. **Applied Physics Letter**, 62, 1995.

[71] Takenaka T. and Nagata, H. (2005). Current status and prospects of lead-free piezoelectric ceramics. **Journal of Europium Ceramic Societies**, 25, 2693.

[72] Chu, B. J., Chen, D. R., Li, G. R. and Yin, Q. R. (2002). Electrical properties of $Na_{0.5}Bi_{0.5}TiO_3$-$BaTiO_3$ ceramics. **Journal of European Ceramics Societies**, 22, 2115.

[73] Lin, Y., Zhao, S., Cai, N., Wu, J., Zhou X. and Nan, C.W. (2003). Effects of doping $Eu_2O_3$ in the phase transformation and piezoelectric properties of $(Bi_{0.5}Na_{0.5})TiO_3$-based ceramics. **Meterials Sciences Engineering B**, 99, 449.

[74] Herabut, A. and Safari, A. (1997). Processing and electromechanical properties of $(Bi_{0.5}Na_{0.5})_{(1-1.5x)}La_xTiO_3$. **Journal American Ceramic Socities**, 80, 2954.

[75] Takenaka, T. and Nagata H. (1997). Lead-free piezoelectric ceramics of $(Bi_{0.5}Na_{0.5})TiO_3$ $0.5(Bi_2O_3 \cdot Sc_2O_3)$ system. **Japanese Journal Applied Physics**, 36, 6055.

[76] Zhou, C. and Liu, X. (2008). Dielectric and piezoelectric properties of bismuth-containing complex perovskite solid solution of $Bi_{0.5}Na_{0.5}TiO_3$–$Bi(Mg_{0.7}Nb_{0.3})O_3$. **Journal Materials Sciences**, 43, 1016.

[77] Zhou, C. and Liu, X. (2008). Dielectric and piezoelectric properties of $Bi_{0.5}Na_{0.5}TiO_3$–$BaNb_2O_6$lead-free piezoelectric ceramics. **Journal Materials Sciences Materials Electronic**, 19, 29.

[78] Sakata, K. Takenaka, T. and Naitou, Y. (1992). Phase relations, dielectric and piezoelectric properties of ceramics in the system $(Bi_{0.5}Na_{0.5})TiO_3$–$PbTiO_3$. **Ferroelectrics**, 131, 219.

[79] Zou, M., Fan, H., Chen, L. and Yang, W. (2010). Microstructure and electrical properties of (1-x)$[0.82Bi_{0.5}Na_{0.5}TiO_3$-$0.18Bi_{0.5}K_{0.5}TiO_3]$-$xBiFeO_3$ lead-free piezoelectric ceramics. **Journal Alloy and Compound**, 10, 1.

[80] Hussain, A., Ahn, C.W., Ullah, A. and Lee, J. S., Kim, I.W. (2010). Dielectric, ferroelectric and field-induced strain behavior of $K_{0.5}Na_{0.5}NbO_3$-modified $Bi_{0.5}(Na_{0.78}K_{0.22})_{0.5}TiO_3$ lead-free ceramics. **Ceramics International**, 12, 00090.

[81] Singh, A. and Chatterjee, R. (2011). Structure, electrical, and strain properties of stoichiometric 1-x-y$(Bi_{0.5}Na_{0.5})TiO_3$–x$(Bi_{0.5}K_{0.5}TiO_3)$-y$(Na_{0.5}K_{0.5})NbO_3$. **Journal of Applied Physic**, 109, 024105.

[82] Lin, D., Zheng, Q., Xu, C. and Kwok, K.W. (2008). Structure, electrical properties and temperature characteristics of $Bi_{0.5}Na_{0.5}TiO_3$ –$Bi_{0.5}K_{0.5}TiO_3$ – $Bi_{0.5}Li_{0.5}TiO_3$ lead-free piezoelectric ceramics. **Applied Physics A**, 93, 549.

[83] Hiruma, Y., Nagata, H. and Takenaka, T. (2009). Depolarization temperature and piezoelectric properties of $(Bi_{0.5}Na_{0.5})TiO_3$ –$(Bi_{0.5}Li_{0.5})TiO_3$ – $(Bi_{0.5}K_{0.5})TiO_3$lead-free piezoelectric ceramics. **Ceramics International**, 35, 117.

[84] Swartz, S. L. and Shrout, T. R. (1982). Fabrication of Perovskite Lead Magnesium Niobate. **Materials Research Bulletin**, 17, 1245.

[85] Lee, W. E. and Rainforth, W. M. (1994). **Ceramic Microstructures Property Control by Processing**. London: Chapman & Hall.

[86] Flewitt, P. E. J. and Wild, R.K. (1985). **Microstructure Characterization of Materials and Alloys**, London: I.O. Metals.

[87] Shi, J., Fan, H. and Li, Z. (2010). Elelctromechanical properties and microstructure evolution of BNT-BT piezoelectric ceramics. **Ferroelectrics**, 404, 93.

[88] Kounga, A.B., Zhang, S.T., Jo, W., Granzow, T. and Rodel, J. (2008). Morphotropic phase boundary in (1-x)$Ba_{0.5}Na_{0.5}TiO_3$–x$K_{0.5}Na_{0.5}NbO_3$ lead-free piezoceramics. **Applied Physics Letter**, 92, 222902.

[89] Thongtha, A. Angukased, K. and Bongkarn, T. (2010). Fabrication of $(Ba_{1-x}Sr_x)(Zr_xTi_{1-x})O_3$ ceramics prepared using the combustion technique. **Smart Material Structure**, 19, 12400.

[90] Wonggmaneerung, R., Yimnirun, R. and Ananta S. (2006). Effects of milling time and calcinations conditions on phase formation and particle size of lead titanium nanopowders prepared by vibro-milling. **Material Letter**, 60, 2666.

[91] Konig, J., Spreitzer, M., Jancar, B., Surorov, D., Samardzjja, Z. and Popovic, A. (2009). The thermal decomposition of $K_{0.5}Bi_{0.5}TiO_3$ ceramics. **Journal of European Ceramics Societies**, 29, 1695.

[92] Hiruma, Y., Nagata, H. and Takenaka, T. (2008). Phase diagrams and electrical properties of $(Bi_{1/2}Na_{1/2})TiO_3$-based solid solutions. **Journal of Applied Physics**, 104, 124106.

[93] Xiao, D.Q., Lin, D.M., Zhu, J.G. and Yu, P. (2006). Investigation on the design and synthesis of new systems of BNT-based lead-free piezoelectric ceramics. **Journal of Electroceramics**, 16, 271.

[94] Lei, N., Zhu, M., Yang, P., Wang, L. Wang, L. Hou, Y. and Yan. H. (2011). Effect of lattice occupation behavior of $Li^+$ cations on microstructure and electrical properties of $(Bi_{1/2}Na_{1/2})TiO_3$-based lead-free piezoelectric ceramics. **Journal of Applied Physics**, 109, 054102.

[95] Rahman, J., Hussain, A., Maqbool, A., Kim, J.S., Song, T.K., Kim, J.S., Song, T.K., Lee, J.H., W.J. Kim and M.H. Kim. (2013). Ferroelectric and impedance response of lead-free $(Bi_{0.5}Na_{0.5})TiO_3$–$BaZrO_3$ piezoelectric ceramics. **Materials Science and Engineering**, 60, 012043.

[96] Sumang, R. and Bongkarn, T. (2013). The influence of firing temperatures on the crystal structure, microstructure and dielectric properties of $0.79Bi_{0.5}Na_{0.5}TiO_3$-$0.18Bi_{0.5}K_{0.5}TiO_3$-$0.03BiFeO_3$ ceramics prepared via the combustion technique. **Ferroelectrics**, 454, 152.

[97] Xiang, P.H., Takeda, H. and Shiosaki, T. (2008). Characterization of manganese-doped $BaTiO_3$-$(Bi_{1/2}Na_{1/2})TiO_3$ positive temperature coefficient of resistivity ceramics using impedance spectroscopy. **Journal of Applied Physics**, 103, 064102.

[98] Wang, F., Leung, C.M., Tang, Y., Wang T. and Shi, W. (2013). Composition induced structure evolution and large strain response in ternary $Bi_{0.5}Na_{0.5}TiO_3$–$Bi_{0.5}K_{0.5}TiO_3$–$SrTiO_3$ solid solution. **Journal of Applied Physics**, 114, 164105.

[99] Dai, Y.J., He, A.A., Lao X. and Zhang, S.Z. (2014). The relationship between phase structure and electrical properties in (1-x)($Bi_{0.5}Na_{0.5}TiO_3$–$Ba_{0.5}K_{0.5}TiO_3$–$BaTiO_3$)-x$K_{0.5}Na_{0.5}Nb_{0.5}O_3$ quaternary lead-free piezoelectric Ceramics. **Journal of American Ceramics Society**, 97, 1183.

[100] Zhang, S.T. Hounga, A.B. Aulbach, E. Ehrenberg, H. and Rodel, J. (2007). Giant strain in lead-free piezoceramics $Bi_{0.5}Na_{0.5}TiO_3$–$BaTiO_3$–$K_{0.5}Na_{0.5}NbO_3$ system. **Applied Physics Letter**, 91, 112906.

[101] Yao, Z., Liu, H., Chen L. and Cao, M. (2009). Morphotropic phase boundary and piezoelectric properties of $(Bi_{1/2}Na_{1/2})$1-x$(Bi_{1/2}K_{1/2})xTiO_3$-$0.03(Na_{0.5}K_{0.5})NbO_3$ ferroelectric Ceramics. **Materials Letters**, 63, 547.

[102] Zhang, S.T. Kounga, A.B. Aulbach, E. Granzow, T. Jo, W. Kleebe, H.J. and Rodel, J. (2008). Lead-free piezoceramics with giant strain in the system $Bi_{0.5}Na_{0.5}TiO_3$–$BaTiO_3$–$K_{0.5}Na_{0.5}NbO_3$. I. Structure and room temperature properties. **Journal of Applied Physics**, 103, 034107.

[103] Kounga, A.B., Zhang, S.T., Jo, W., Granzow, T. and Rodel, J. (2008). morphotopic phase boundary in (1-x)$B_{0.5}N_{0.5}TiO_3$-x$K_{0.5}Na_{0.5}NbO_3$ lead-free piezoelectric. **Applied Physics Letter**, 92, 222902.

[104] Dittmer, R., Gobeljic, D., Jo, W., Shvartsman, V.V., Lupascu, D.C., Jones, J.L. and Rodel, J. (2014). Ergodicity reflected in macroscopic and microscopic field-dependent behavior of BNT-based relaxors. **Journal of Applied Physics**, 115, 084111.

[105] Seifert, K.T.P.Jo, W. and Rodel, J. (2010). Temperature-Insensitive large strain of $(Bi_{1/2}Na_{1/2})TiO_3$-$(Bi_{1/2}K_{1/2})TiO_3$-$(K_{0.5}Na_{0.5})NbO_3$ lead-free piezoceramics. **Journal of American Ceramic Societies**, 93, 1392.

[106] Mgbemere, H.E., Herber R.P. and Schneider, G. A. (2009). Investigation of the dielectric and piezoelectric properties of potassium sodium niobate ceramics close to the phase boundary at $(K_{0.35}Na_{0.65})NbO_3$ and partial substitutions with lithium and antimony. **Journal of the European Ceramic Society**, 29, 3273.

[107] Laoratanakul, P., Yimnirun, R. and Wongsaenmai, S. (2011). Phase formation and dielectric properties of bismuth sodium titanate-potassium sodium niobate ceramics. **Current Applied Physics**, 11, S161.

[108] Yao, Z. Liu, H. Chen L. and Cao, M. (2009). Morphotropic phase boundary and piezoelectric properties of $(Bi_{1/2}Na_{1/2})1\text{-}x(Bi_{1/2}K_{1/2})xTiO_3\text{-}0.03(Na_{0.5}K_{0.5})NbO_3$ ferroelectric ceramics. **Materials Letters**, 63, 547.

[109] Sapper, E., Novak, N. Jo, W. Granzow T. and Rodel, J. (2014). Electric-field-temperature phase diagram of the ferroelectric relax or system $(1\text{-}x)Bi_{1/2}Na_{1/2}TiO_3\text{-}xBaTiO_3$ doped with manganese. **Journal of Applied Physics**, 115, 194104.